

**ENGINEERING CELLULOSE NANOFIBERS FOR BETTER
PERFORMANCE AS NANOCOMPOSITES AND ITS IMPLICATIONS
FOR ADVANCED MATERIALS**

by

Miran Mavlan

A Dissertation

Submitted to the Faculty of Purdue University

In Partial Fulfillment of the Requirements for the degree of

Doctor of Philosophy



Department of Chemistry

West Lafayette, Indiana

August 2019

THE PURDUE UNIVERSITY GRADUATE SCHOOL
STATEMENT OF COMMITTEE APPROVAL

Dr. Alexander Wei, Chair

Department of Chemistry

Dr. Christopher Uyeda

Department of Chemistry

Dr. Corey Thompson

Department of Chemistry

Dr. Jefferey Youngblood

Department of Material Engineering

Approved by:

Dr. Christine Hrycyna

Head of the Graduate Program

Dedicated to my wife, my daughter and my parents

ACKNOWLEDGMENTS

“A ship maybe safe at shore, but that is not what it is built for” – Albert Einstein

In many ways the pursuit of a goal is not only about arriving at the destination, but equally important is the transformation one undergoes along the journey. My evolution from a student to a researcher is in thanks to three people who without their aid I would have certainly failed. My wife, Emel Kasgarli, whose patience and encouragement for a husband 2000 mile away to achieve his dreams while bearing the burden of running a home, caring for our daughter, and maintaining a full-time work load at UCLA Medical Residency is second to none. Thank you “Jenim” for bearing such a heavy load. Secondly, my parents, Mavlan Yasin and Gulbahar Mamut who taught me to value the importance of seeking knowledge. My dad who taught me that all the brains and bronze will never add up to simple persistence and that hard work and *consistent* hard work are *not* the same thing. My mom, who upon hearing that advice added “that is true, but persistence without passion makes you the walking dead.” Lastly, my advisor Professor Alexander Wei, who by offering me freedom to explore my ideas while challenging me every step of the way, helped my metamorphosis into an independent and confident thinker. I learned 3 lessons from him which are more precious than any scientific fact learned: (1) never fear to venture into unexplored territory (2) a good scientist is a skeptical one (3) regardless of success a systematic experiment will always give useful data.

My committee members, Dr. Uyeda, Dr. Thompson and Dr. Youngblood, who with their help allowed this thesis to be improved far beyond my own powers. My lab members, who filled most of my memories at Purdue with laughter and joy. Their companionship will be hard to replace.

TABLE OF CONTENTS

LIST OF TABLES.....	7
LIST OF FIGURES	8
LIST OF EQUATIONS	11
CHAPTER 1. EXTRACTION, PROPERTIES AND APPLICATIONS OF CELLULOSE NANOFIBERS	14
1.1 Introduction to the Guiding Principles of Green Chemistry and Cellulose Structure	14
1.2 Extraction of Cellulose Nanofibers (CNF), Cellulose Nanocrystals (CNC), and their Properties	17
1.3 Applications of Cellulose Nanofiber Based Materials.....	24
CHAPTER 2. MECHANOCHEMICAL GRAFTING OF CELLULOSE NANOFIBERS	28
2.1 Introduction to Mechanochemistry	28
2.2 Mechanochemical Grafting of Cellulose Nanofibers and Degree of Substitution Analysis	35
2.3 Experimental.....	39
2.4 Results and Discussion	40
2.5 Conclusion	50
CHAPTER 3. THE ROLE OF CO-SOLVENT IN THE LYOPHILIZATION OF CELLULOSE NANOFIBERS	52
3.1 Introduction to different drying techniques for CNFs	52
3.2 Cake Formation/TBA: Importance and Interpretation.....	56
3.3 Experimental.....	60
3.4 Results and Discussion	61
3.5 Conclusion	74
CHAPTER 4. STUDIES ON the SUPERHYDROPHOBIC properties OF fatty acid-esterified CELLULOSE NANOFIBERS.....	75
4.1 Introduction to superhydrophobic materials	75
4.2 Generating Cellulose Nanomaterials with Hydrophobic Surfaces	78
4.3 Experimental.....	79
4.4 Results and Discussion	79

4.5 Conclusion	87
REFERENCES	88
VITA.....	98
PUBLICATIONS.....	99

LIST OF TABLES

Table 1.1 The 12 guiding principles of Green Chemistry and their adages ²	15
Table 2.1 Some early mechanochemical conditions.....	43
Table 2.2 Optimization of conditions using high-speed ball mill (Zr = Zirconium balls, SS = stainless steel, Alum. = alumina).....	44
Table 2.3 DS values obtained and volume and ratio of washing solvents used for various compounds	47
Table 3.1 Relative mass changes of air-dried CNF samples after dewatering with five acetone washes (initial wet mass = 94 g).....	62
Table 3.2 BET measurements of freeze-dried CNFs, as a function of initial TBA wt% prior to lyophilization. Data acquired by Taehoo Chang.....	71
Table 3.3 DS value of esterified CNFs (lyophilized with 10% TBA as cosolvent)	73
Table 4.1 Static contact angles for spray-coated CNG thin films on PET substrates. Data collected by Taehoo Chang.	83
Table 2. Estimates of soluble reducing sugars in filtrates using the modified BCA assay.....	104

LIST OF FIGURES

Figure 1.1 Structure of cellulose with hydrogen bonding within and between chains (left) and 1→4 glycosidic linkage of cellobiose unit (right)	17
Figure 1.2 Isolation of nanocellulose materials and regions of crystallinity	19
Figure 1.3 Examples of colloidal CNF suspensions: (A) sedimentation, (B) flocculation, (C) stable dispersion	20
Figure 1.4 Some Examples of Surface Grafting of Cellulose.....	21
Figure 1.5 Acid digestion of CNFs into CNCs and their respective dimensions	23
Figure 1.6 Mud–straw composites as a macroscopic analogy to nanocellulose–polymer composites.	25
Figure 1.7 3D printing onto CNF substrates for microfluidic applications	27
Figure 2.1 Planetary mill (A), Tumbling ball mill (B), and Vibrational mixer (C).....	29
Figure 2.2 Illustrations of (A) hot-spot theory (B) plasma model	31
Figure 2.3 Milling media available for mechanochemical grinding.....	32
Figure 2.4 General trends of regions during a milling reaction.....	35
Figure 2.5 CDI-mediated CNF surface functionalization. hbm = horizontal ball milling.....	38
Figure 2.6 (A) Free sugar concentration detected for various samples (B) Wash cycles and detected sugar amounts	41
Figure 2.7 MC conditions using a planetary ball mill. Significant degradation or charring of reaction materials was observed.	43
Figure 2.8 Horizontal ball milling with Zr balls in NALGENE bottles (30 rpm)	45
Figure 2.9 IR spectra of CNFs esterified with lauric (C12) and stearic (C18) acid after low-speed milling.....	46
Figure 2.10 Scope of compounds grafted onto CNFs under mechanochemical conditions, with carbonyl ester stretches.	46
Figure 2.11 Examples of coated balls that arise for vicious starting materials.....	48
Figure 2.12 Functionalized CNF at 1 w/v% concentration in various solvents (A) Stearoylated CNF; (B) Furoylated CNF	49
Figure 2.13 Surface-modified CNFs dispersed in various solvents, after 24 hours. Vials on the left were prepared using standard freeze-dried CNFs; Vials on the right were prepared using CNFs freeze-dried from aqueous TBA solutions.....	51

Figure 3.1 (A) Hornification is the irreversible collapse of CNF fibers during the drying process (B) Fiber bundling and pore size reduction as the result of hornification ⁷⁷	53
Figure 3.2 Diagram of the phase changes involved in FD (blue arrow) and SCD (red arrow)	55
Figure 3.3 Cake appearance as an indicator of freeze-drying quality. ⁹⁷	58
Figure 3.4 Dewatering of acetone-treated CNFs resulted in hardened flakes that resisted further processing	62
Figure 3.5 Shrinkage and curling of air- and oven-dried CNFs, dewatered by acetone washing	63
Figure 3.6 Vacuum drying of dewatered CNF samples under a mechanical load.....	64
Figure 3.7 <i>Left</i> , lyophilized CNF samples taken out at different time periods (1–4 days). <i>Right</i> , porous and hardened CNF cake after partial lyophilization then drying under ambient conditions.	65
Figure 3.8 (A) Benchtop (manual) kitchen grinder used to shred freeze-dried CNF into coarse grains; (B) Freeze-dried CNF before grinding; (C) CNFs after being subjected to coarse and fine shredding by manual grinder; (D) Further reduction of CNF grains using electric coffee grinder	66
Figure 3.9 Collapse and shrinkage of FD-CNF cakes prepared from different solvent mixtures: <i>Left</i> , untreated CNF; <i>middle</i> , 5 wt% TBA; <i>right</i> , 20% TBA	67
Figure 3.10 Colloidal stability of CNFs redispersed in water after freeze drying. Samples were allowed to stand for 24 hours after initial dispersion by sonication. <i>Left</i> , after FD with 56 wt% NBA; <i>middle</i> , after FD with 43 wt% TBA; <i>right</i> , no co-solvent added	67
Figure 3.11 CNF cakes after freeze-drying from aqueous slurries containing 10 to 35 wt% TBA.	68
Figure 3.12 Appearance of FD-CNF cakes from aqueous slurries containing 10–30 wt% NBA	69
Figure 3.13 SEM images of freeze-dried CNFs. <i>Upper left</i> , FD-CNF lyophilized from 10 wt% TBA slurry; <i>upper right</i> , FD-CNF lyophilized from 20 wt% TBA slurry. Bottom, FD-CNF without TBA treatment. Images taken by Taehoo Chang.....	70
Figure 3.14 Images (5 cm x 5 cm) of cast films prepared from 1 wt% laurylated CNF in chloroform. <i>Left</i> , prepared using CNFs lyophilized from water (untreated); <i>right</i> , prepared using CNFs lyophilized from slurries with 20 wt% TBA.....	72
Figure 4.1 (Above) Contact angles for hydrophilic, hydrophobic and superhydrophobic (SHP) surfaces supporting a water droplet. (Below) Photo of a water droplet on a SHP-CNF surface..	76
Figure 4.2 The two physical models used to explain wetting phenomena at the air/liquid/solid interface.....	77
Figure 4.3 <i>Above</i> , stearyl versus oleyl chains grafted on CNF surfaces; <i>below</i> , disk of oleyl- CNF after filtering and drying	80
Figure 4.4 Freely moving water droplets on oleylated CNF disk.....	81

- Figure 4.5. Spray coating of oleyl-CNF onto PET film; a SHP coating was formed after several passes. SHP demonstrations were performed by placing the coated PET at an incline. 82
- Figure 4.6 Water droplet dispensed onto functionalized CNF surfaces. Photos taken by Taehoo Chang. 83
- Figure 4.7 SEM image of oleyl-CNFs spray-coated onto PET substrate. Image taken by Taehoo Chang. 84
- Figure 4.8 (A) Olelylated CNF mounted on a glass slide showing SHP behavior; (B) pressing sample with unwashed thumb; (C) loss of SHP due to contaminated surface; (D) exfoliation of surface with Scotch tape; (E) restoration of SHP using exfoliated sample on glass slide, and also reverse side of tape..... 85
- Figure 4.9 (A) SEM image of OA-CNF after compression with gloved thumb; (B) recovery of surface roughness after exfoliation. Images taken by Taehoo Chang. 86
- Figure 5 MS/MS Result from selected MALDI Ions. Dextrose is pointed out to show the proximity of the detected fragments to a single ring saccharide. 109

LIST OF EQUATIONS

Equation 1 DS calculation by weight change before and after surface modification.....	37
---	----

ABSTRACT

Author: Mavlan, Miran,. PhD

Institution: Purdue University

Degree Received: August 2019

Title: Engineering Cellulose Nanofibers for Better Performance as Nanocomposites and its Implications for Advanced Materials

Committee Chair: Alexander Wei

In recent decades there has been great interest to produce novel bio-based composites to reduce carbon footprint without sacrificing the necessities that society demands. To achieve a more sustainable future, research in cellulose biopolymers has risen to the forefront. Impressive mechanical, thermal and optical properties along with its abundant biomass has made nanocellulose (NC) the subject of intense research in the area of electronics, drug delivery, sensors, selective filters, and structural materials, to name a few. The practical utility of any cellulose-based materials requires a more complete understanding of how the fundamental structure affects final performance. This thesis examines several avenues to obtain novel materials by considering processing parameters and preparation methods for working with raw nanocellulose materials, and mechanochemical approaches for surface grafting to obtain modified CNs with improved dispersion in organic media. Lastly, the synergy between the two studies and its impact on advanced materials and nanocomposites is discussed.

The low cost and wide availability of cellulose nanofibers (CNF), a refined form of cellulose microfibrils, make these an ideal starting material for our studies. However, the aggregated states of freeze-dried CNFs hinder its use as an additive for reinforcing polymer blends or functional films. The use of *tert*-butyl alcohol (TBA) as a stabilizer in pharmaceutical drugs has been well studied for its effectiveness in facilitating redissolution and extending product shelf life.

Lyophilization of aqueous CNF slurries treated with various amounts of TBA produced a more porous material that could be redispersed with superior colloidal stability relative to untreated freeze-dried CNFs. Furthermore, CNFs lyophilized from aqueous TBA mixtures could be subjected to mild mechanochemical reactions (horizontal ball milling) to produce esterified nanofibers with high degrees of substitution (DS) and good dispersibility profiles in organic solvents. This solventless technique allowed for a variety of carboxylic acids to be grafted onto CNF surfaces. Finally, investigations of new materials with technological utility have been explored using networks of CNFs modified with oleic acid. These can be cast into superhydrophobic (SHP) films having a hierarchical structure characteristic of a self-similar material, with a wettability comparable to that of the lotus leaf. The SHP surface can also be regenerated after surface fouling or physical damage.

CHAPTER 1. EXTRACTION, PROPERTIES AND APPLICATIONS OF CELLULOSE NANOFIBERS

1.1 Introduction to the Guiding Principles of Green Chemistry and Cellulose Structure

Sustainability has often been defined by many parameters and just like its definition the means by which to obtain it has always been changing. Prior to any real scientific descriptions for what parameters constitute sustainability, the debate had always been in the political arena. There arose a distinct argument from an *environmental* point of view versus advocates of *economic* growth, who celebrated industrial machinery as the engine of progress that should not be tampered with at any cost.¹ The maturation of the ideas belonging to both these areas of concern made it clear that integration (or synergy) is the solution and that economic growth need not be stifled by environmental concerns. In fact, the development of “green chemistry” has the potential for new areas of innovation and growth previously not considered. Paul Anastas and John Warner developed the 12 guiding principles² for making a process more “green” or sustainable (Table 1.1), and each category has seen intensive research and development since its inception.²

Table 1.1 The 12 guiding principles of Green Chemistry and their adages²

Guiding Principle	Adage
1. Waste Prevention	The prevention of waste is better than containment
2. Atom Economy	Reduce waste not just on the macro level, but also the molecular level
3. Less Hazardous Synthesis	Choose shorter and safer routes with the environment and scientist in mind
4. Design Benign Chemicals	Reagents should be <u>designed</u> to be less toxic
5. Benign Solvents & Auxiliaries	Always try to avoid solvents, but if needed judicious selection of a <u>green</u> solvent to be used a <u>minimum</u> amount
6. Design for Energy Efficiency	If possible avoid high or low temperature and pressure conditions. Ambient reactions are best
7. Use of Renewable Feedstock	When possible (availability and cost) plant based raw materials should be chosen over petroleum based
8. Reduce Derivatives	Simplify synthesis as much as possible by avoiding unnecessary steps (e.g. no protecting groups)
9. Catalytic over Stoichiometric	When possible always choose catalytic over stoichiometric conditions
10. Design for Degradation	Plan ahead for choosing reagents and conditions with biodegradable byproducts
11. Real Time Analysis of Pollution	Monitor reactions to minimize or remove hazardous byproducts before build up
12. Inherently Benign Chemistry for Accident Prevention	An inherently safer strategy that may give moderate yield is better than a high yielding hazardous route

Cellulose is a biorenewable feedstock that makes up ~40% of all terrestrial biomass, with an estimated production of 7.5×10^{10} tons per year.³ As the most abundant biopolymer on earth, cellulose is produced by various sources besides wood, including numerous plant species (hemp,⁴ sugar beets,⁵ flax,⁶ and cotton,⁷ which is >90% cellulose), bacterial species (*Acetobacter*,⁸ *Alcaligenes*,⁹ *Pseudomonas*,¹⁰ and *Sarcina*¹¹), and diverse marine organisms such as tunicates.¹² Interestingly, nature produces cellulose by diverse biosynthetic pathways that yield various polymorphs of this bountiful amphiphilic polymer. For example, cellulose produced from bacteria will have a different form than that of derived from wood.¹³ Natural sources of crystalline cellulose, once extracted, are termed Cellulose I, which is characterized by its triclinic unit cell. Cellulose I

can be converted to the thermodynamically more stable Cellulose II (monoclinic unit cell) via mercerization (alkali treatment).¹⁴ However, regardless of origin and macrostructure, all types of crystalline cellulose have remarkable mechanical features, which arise from its molecular properties and bonding profile.

Cellulose is a simple homopolysaccharide that consists of linear chains of D-glucose dimers linked in repeating β -(1 \rightarrow 4) units, termed cellobiose, which commonly number between 10,000 and 15,000 units (Figure 1.1).¹⁵ The polymer can be stacked either parallel or antiparallel (depending on the source) with stabilization by intermolecular hydrogen bonding due to its high density of free hydroxyls. There are several distinguishing features that arise from this molecular arrangement: (1) each glucose unit is oriented 180° from its neighbor with all secondary hydroxyls oriented in equatorial positions, (2) each glucose unit has 3 hydroxyl groups available for hydrogen bonding interactions, and (3) the primary (C6) hydroxyl groups, which are most amenable to chemical modifications, are oriented upward and away from interstitial space in *every other* glucose unit. The hydrogen bonding and chain stacking interactions result in mostly crystalline domains separated by disordered regions. These two regions greatly affect the mechanical properties (e.g. Young's modulus, tensile strength, and toughness) and react differently to acid hydrolysis conditions.

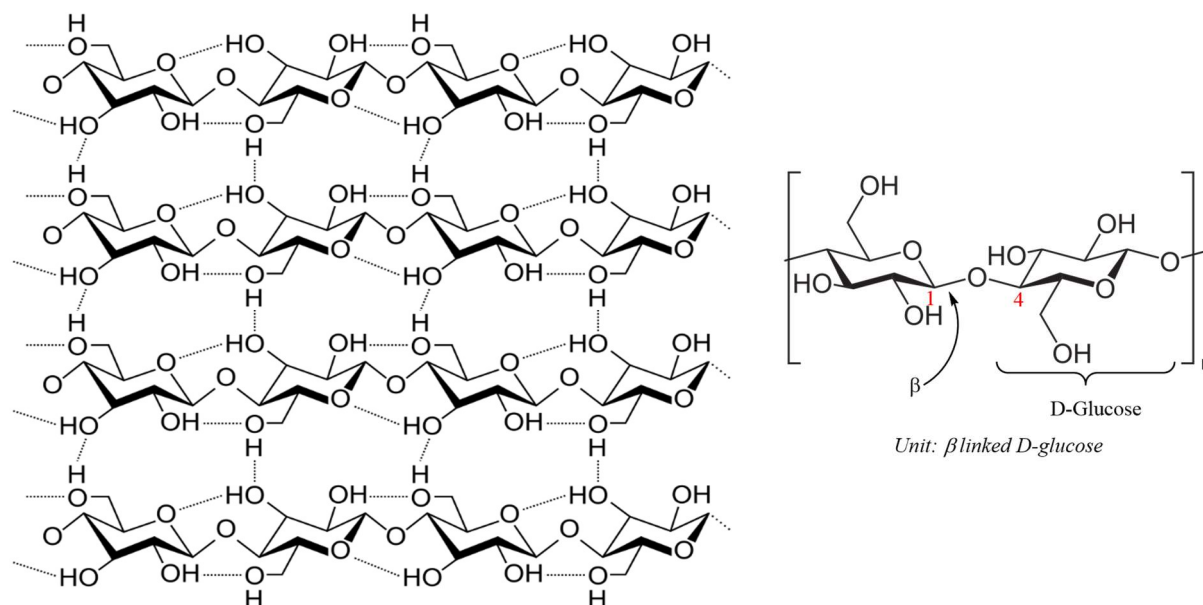


Figure 1.1 Structure of cellulose with hydrogen bonding within and between chains (left) and 1→4 glycosidic linkage of cellobiose unit (right)

1.2 Extraction of Cellulose Nanofibers (CNF), Cellulose Nanocrystals (CNC), and their Properties

Wood-derived cellulose represents a primary source of renewable biomass and is also the source of CNFs used in our studies. Wood is available in large quantities at low cost; its societal impact is evident from its long history and ubiquitous role in the design of human habitats.¹⁶ Cellulose in wood is hierarchically structured down to the nanoscale.¹⁷ Cellulose is converted into wood pulp using chemical processes on the multi-ton scale, resulting in aqueous slurries of microfibrils of high purity.¹⁸ The cellulose microfibrils have lengths up to 3 mm and widths up to 50 μm .¹⁹ Traditional methods to isolate CNFs from wood pulp include: (1) mechanical separation such as grinding to induce cell wall breakdown, (2) treatment with alkali solutions to remove surface lignin and to ease the separation of fibers from bulk pulp, and (3) homogenization of the pulp suspension by filtration through a grooved pore under high pressure, where shearing helps

isolate the nanomaterial.²⁰ Regardless of method, the resulting CNFs are typically micrometers in length with widths in the range of 5–20 nm.

CNFs are essentially a network of fibrous strands with alternating crystalline and non-crystalline regions (Figure 1.2). The assortment of the fibers best resembles that of a tangled spider's web with some portions that are straight and aligned and others in randomly entangled bundles. The diameter of the bundles can be as large as 100 nm depending on the degree of agglomeration.²¹ The dimensions of the bundled fibers are large enough to produce strong light scattering, which accounts for its characteristic opacity in solution or when cast into solid films. However, CNFs can be manufactured into transparent paper by mechanically pressing wet CNF fiber sheets with vacuum filtration to eliminate air bubbles and decrease light scattering by closing the interstitial gaps.²²

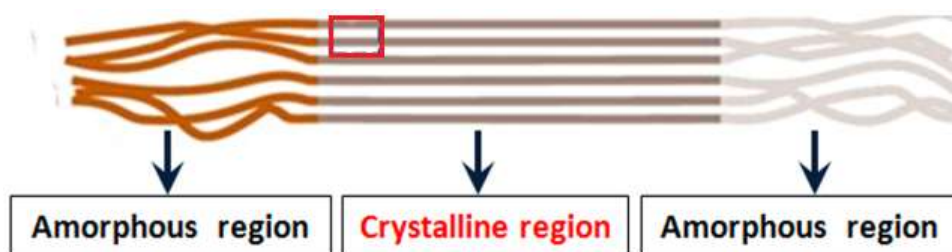
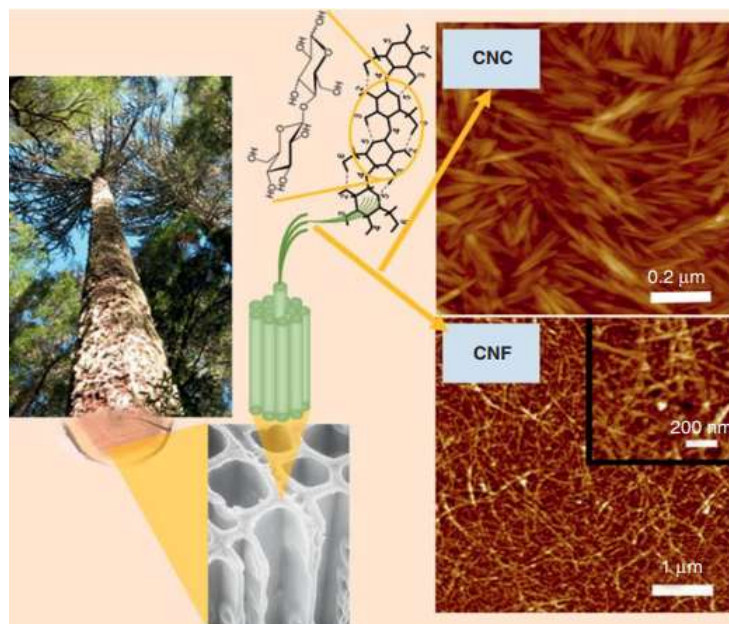


Figure 1.2 Isolation of nanocellulose materials and regions of crystallinity

CNFs can be dispersed in a solution as a suspension whose stability depends on multiple factors. Much research has been dedicated toward controlling CNF dispersibility and stability in both aqueous and organic solvents.²³ Colloidal stability of NC solutions (Figure 1.3) is characterized by the rate of sedimentation and flocculation,²⁴ the importance of which will be discussed in more detail in the following section (Section 1.3).

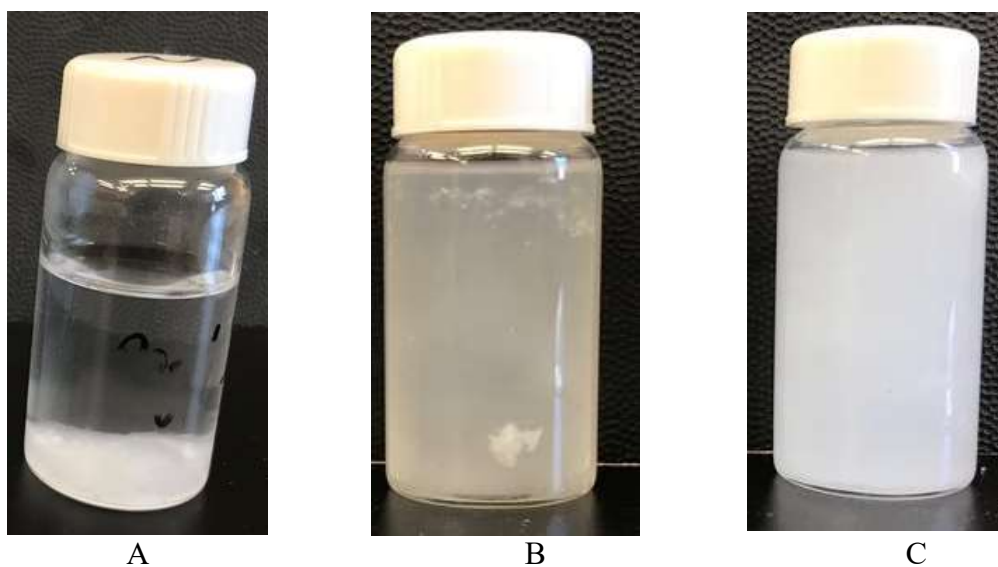


Figure 1.3 Examples of colloidal CNF suspensions: (A) sedimentation, (B) flocculation, (C) stable dispersion

The techniques used to improve dispersion can be divided roughly into two categories: methods that utilize covalent surface modification by grafting organic molecules (or polymers) onto the available hydroxyl groups, and methods that rely on mechanochemical methods with the optional use of surfactants, disk grinding, cryocrushing, and high-energy homogenization.²⁰ Surface grafting is performed to battle the natural tendency of CNFs to agglomerate; conversion of free hydroxyls to esters, amides, carbamates, and ethers is a commonly employed strategy (Figure 1.4). The degree of substitution (DS) is often characterized by FTIR or solid-state carbon-13 NMR²⁵.

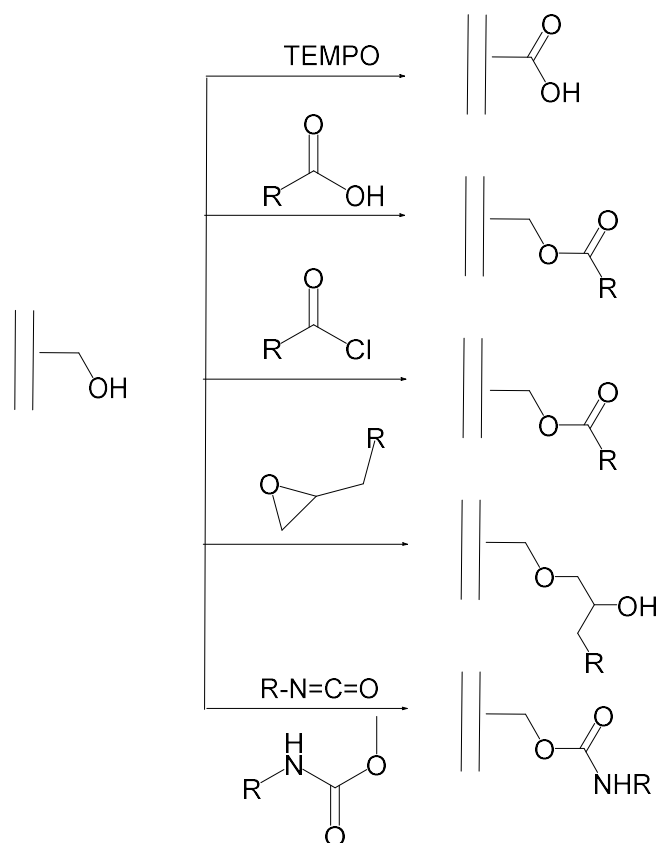


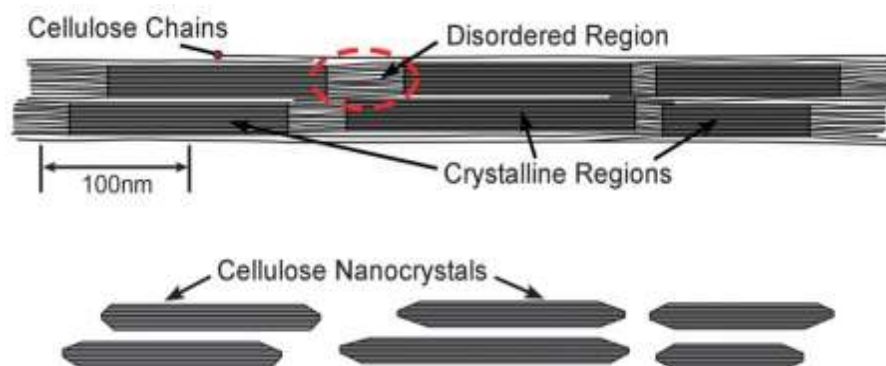
Figure 1.4 Some Examples of Surface Grafting of Cellulose

DS defines the extent to which the surface hydroxyl groups of an anhydroglucose unit (AGU) has been functionalized; methodology, analysis, and implications will be discussed in more detail in Chapter 2. DS values as high as 2.0 per AGU and low as 0.1 have been reported.²⁶ Another category of controlling dispersion is not by grafting any moieties onto the CNF surface, but by direct oxidation of exposed C6 hydroxyls with TEMPO²⁷ or NaIO₄²⁸ to impart a negative charge onto the CNF surface. The electrostatic repulsion between surfaces into carboxylic acids aids the fibers from aggregating and improves dispersion.

The choice of the functional groups to decorate CNF surfaces must be judiciously selected to complement the solvent the dispersion tests will be performed in. In a seminal work by Youngblood and workers,²⁹ NC was esterified with fatty acid groups (C₁₂, C₁₆ and C₁₈) in a one-

pot synthesis involving in situ polymerization and grafting of polylactic acid onto CNC surfaces. Plots of Hildebrand solubility parameters, which quantifies the energy of molecular interaction (units: $\text{cal}^{1/2} \text{cm}^{-3/2}$), against the *absorbance* of grafted NC suspended in various solvents, produced profiles of colloidal aggregation. Indeed, the type of fatty acid grafted onto the NC surface made a difference depending on the choice of solvent. Furthermore, it was shown that NCs grafted with fatty acids at a low DS value produced transparent solutions when dispersed in organic solvents, as long as the chain length was sufficiently long. The present work will discuss mechanochemical esterification of CNF with fatty acids in Chapter 2.

Cellulose nanocrystals (CNCs), are the products of CNFs treated with strong acids such as H_2SO_4 , HCl or H_2PO_4 (Figure 1.5). The rate of chain hydrolysis in the amorphous regions of CNFs is much faster than for the crystalline portion of isolated fibers, allowing for high yields of CNCs. Post-degradation treatments include washing and dialysis to ensure quality (e.g. removal of any leftover fibers).³⁰ The resulting rod-like nanocrystals (54–88% crystallinity)³¹ are more rigid than CNFs due to the absence of disordered segments. The typical dimensions of a CNC particle are 50 to 500 nm in length and 3 to 50 nm in width.¹⁹ A novel feature of CNCs is their concentration-dependent assembly into cholesteric phases: above a certain concentration threshold, a chiral nematic phase will appear. This fascinating change can be attributed to the minimization of electrostatic interactions between individual CNCs whose surfaces are negatively charged.³²



Type	Length (μm)	Width (μm)	Height (nm)	Crystallinity %
CNF	0.5 – 2	4 – 20	4 – 20	---
CNC	0.05 – 0.5	3 – 5	3 – 5	54 – 88

Figure 1.5 Acid digestion of CNFs into CNCs and their respective dimensions

The absence of harsh acid treatment in producing CNFs hold two major advantages over CNCs, which are *low cost* due to absence of an additional processing step, which leads to an *eco-friendlier* raw material. In terms of performance, a comparative study by Wiesborn et al.³³ was conducted in which CNCs and CNFs were used to reinforce the polyethylene oxide (PEO) matrix. For example, studies on Young's modulus and toughness of the nanocomposite showed an optimal performance at 7 wt% of CNC or CNF content. However, it that was noted that CNF-reinforced PEO had better mechanical properties overall that CNC-reinforced composites, which was attributed to the greater load-bearing capabilities of the entangled CNFs.

1.3 Applications of Cellulose Nanofiber Based Materials

The aforementioned properties of CNFs make them suitable for a wide range of applications. In this brief overview, the scope of CNF utility will be simplified into two broad categories: (1) CNFs as additives to form nanocomposites with improved properties, and (2) applications utilizing monolithic CNF materials. Although, the *majority* of the technological advances comes from the former, some interesting and recent applications of the latter will also be discussed.

The use of additives to form composites with overall improvement in its material performance is not novel by itself. In ancient times it was common practice to mix wet mud (matrix) with straw fibers, which upon drying produced bricks of high durability (Figure 1.6).³⁴ The mechanical load could be increased by the transfer of stress from matrix to fiber, allowing for a tougher material more suitable for homes and infrastructures. In similar fashion, CNF-based *nanocomposites* utilize the relationship between nanocellulose fibers embedded in a polymer, with the objective of improving mechanical properties with a simultaneous decrease in carbon footprint. The high surface area of the nanocellulose fibers allows for maximum interaction with the polymer matrix, which endows improvements in materials performance even at low concentrations without sacrificing the native characteristics of the polymer matrix. Ideally, the ratio of CNF to polymer matrix should be as high as possible without inducing nanofiber aggregation³³ or reducing desirable material properties. For example, adding excess NC to a thermoforming polymer might lower its transition glass temperature (T_g) below a useful threshold.

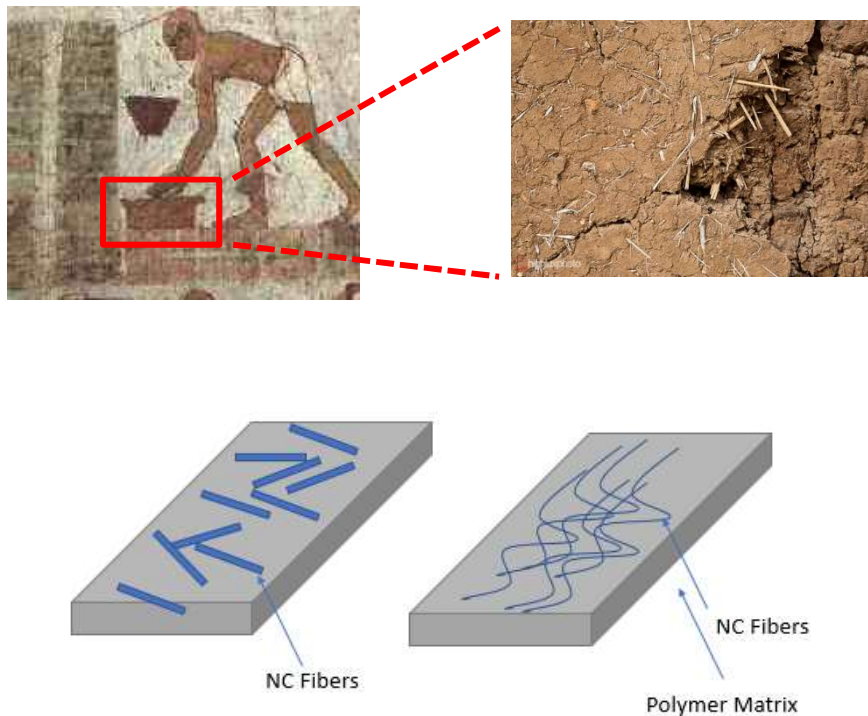


Figure 1.6 Mud–straw composites as a macroscopic analogy to nanocellulose–polymer composites.

Polyethylene (PE), the most ubiquitous synthetic polymer in the world (comprising 35% of total thermoplastics), is the main ingredient in the packaging industry for common items such as shopping bags. A thorough study on the manufacturing of a CNF/PE composite was conducted by Fumiaki et al.³⁵ A twin-screw extruder method was employed to melt-process functionalized CNFs with PE 140–160 °C to yield composites with a significant increase in Young’s modulus (1.20 to 3.32 GPa), and tensile strength (23.4 to 51.2 MPa), and a favorable decrease in coefficient of thermal expansion (CTE) to 72.5 ppm/K (less than 1/3 of pristine PE). The authors noted that the grafting of bulky substituents on the CNF surface such as pivaloyl or *tert*-butylcyclohexylcarboxyl moieties allowed for better dispersibility in PE, relative to acetylated or stearylated CNFs.

In a separate endeavor by Drzal et al,³⁶ CNFs were successfully blended with poly(lactic acid) (PLA), a hydrophobic polymer. Here, polylactide solutions in ethyl acetate were added to an aqueous solution of polysorbate 80, then concentrated to yield a milky emulsion. Subsequent addition of homogenized CNFs to the PLA/polysorbate solution yielded composite sheets having both improved stiffness and strength. Increasing CNF content from 8 to 32 wt% resulted in an increase in both flexural modulus (up to 6 GPa) and strength (up to 110 MPa).

To showcase that CNF-based composites can improve not just mechanical properties but also electrical conductivity, Li et al.³⁷ mixed CNFs with 20 wt% carbon nanotubes (CNTs) under basic conditions to produce a gel film with a complex 3D network, accompanied by a 3-fold improvement in conductivity. The improvement was credited to the many overlapping cellulose nanofibers that supported a high density of electrically conductive CNTs. Future applications of such research will surely find a place in wearable electronics or sensors.

Applications of monolithic CNF materials also exist, and are unique in their own right. For example, CNFs that are extracted using concentrated (12 M) HCl are more crystalline than those generated by mechanical methods, with fibers forming a hierarchical assembly with a parallel arrangement. Wada et al.³⁸ showed that such highly organized CNFs have hydrolytic activity and tested the scope of its reaction against esters, amides and monophosphate bonds of various organic substrates. Biological evidence of the material's ability to decompose virus coatings (wild-type M13 bacteriophage) was also demonstrated. A major selling point of the work was the mild reaction temperature (30 °C) and retention of catalytic activity between pH 5 and 9.

Another good example involves 3D printing, which has evolved from a specialized tool to a readily available technology with the development of interchangeable parts and user-friendly interfaces. Jinho et al.³⁹ used 3D printing to deposit materials directly onto CNF hydrogels (Figure

1.7). The mechanical stability of the CNF substrate allowed for the printed patterns to retain their morphology on the template under drying conditions to form thin films (3D \rightarrow 2D). The films have potential applications in *flexible* paper microfluidics, where the patterned microchannels can direct fluid movement in sensory applications. A successful application of the 2D printed films was demonstrated by the detection of heavy metal ions via a colorimetric assay.



Figure 1.7 3D printing onto CNF substrates for microfluidic applications

In summary, this chapter illustrates some of the methods used in extracting and processing NC materials, the organic chemistry used for surface modification, and a brief survey of applications involving CNFs as nanocomposites or as stand-alone materials. In the following chapters, we will focus on the optimization of freeze-drying conditions that enable CNFs to be processed in the solid state, namely by using solvent-free mechanochemistry for surface modification of CNFs with a high degree of substitution. Several types of fatty-acid modified CNFs are highly miscible in organic solvents and can also be deposited into coatings exhibiting remarkable superhydrophobic properties.

CHAPTER 2. MECHANOCHEMICAL GRAFTING OF CELLULOSE NANOFIBERS

2.1 Introduction to Mechanochemistry

It is a well-established fact that the governing dynamics of chemical processes, whether it is a small-scale reaction setup inside a university lab or an industrial batch reactor inside massive factories, obey fundamental laws of kinetics and thermodynamics. Thermodynamics dictate the possibility for reactions to *even* occur, and kinetics stipulate the speed at which they can proceed at. Spontaneous reactions require no intervention on behalf of the chemist, whereas other reactions require significant activation. Traditional means of applying energy to a chemical system include heat, electricity (electrolytic cells), and light or other forms of electromagnetic radiation. The use of mechanical force to induce chemical change is often overlooked, but it is just as old if not older than the techniques above with records dating back to 315 B.C., prior to the development of modern scientific thought.⁴⁰ It can even be argued that the use of mortar and pestle is the true genesis of mechanochemistry, which can be dated back to the Stone Age.^{40,41}

Mechanochemistry, a term coined in the 19th century⁴², supports at least three guiding principles of green chemistry. First, reactions inside of ball mills, rotary planetary grinders, or vibrational mixers⁴³ (Figure 2.1) are performed dry or use minute amounts of solvent (termed liquid-assisted grinding, or LAG), in accord with Guiding Principle #5. LAG is often used to aid the mechanical reduction of sample particle size. Solvent exclusion can translate into huge cost savings for research laboratories (even more for chemical manufacturing) as solvent cost and waste disposal amounts for much of the cost of production. Second and third, many of the reagents developed for mechanochemical reactions are designed to be safe when exposed to the atmosphere (Guiding Principle #3), and the simplicity of the MC reactors themselves reduces the chances of a

hazardous incident (Guiding Principle #12). In addition to solid reactants, there also exist methods to conduct MC reactions using gaseous reagents.⁴⁴ For more details on the scope of MC reactions, the reader is referred to the excellent review by Wang.⁴⁵

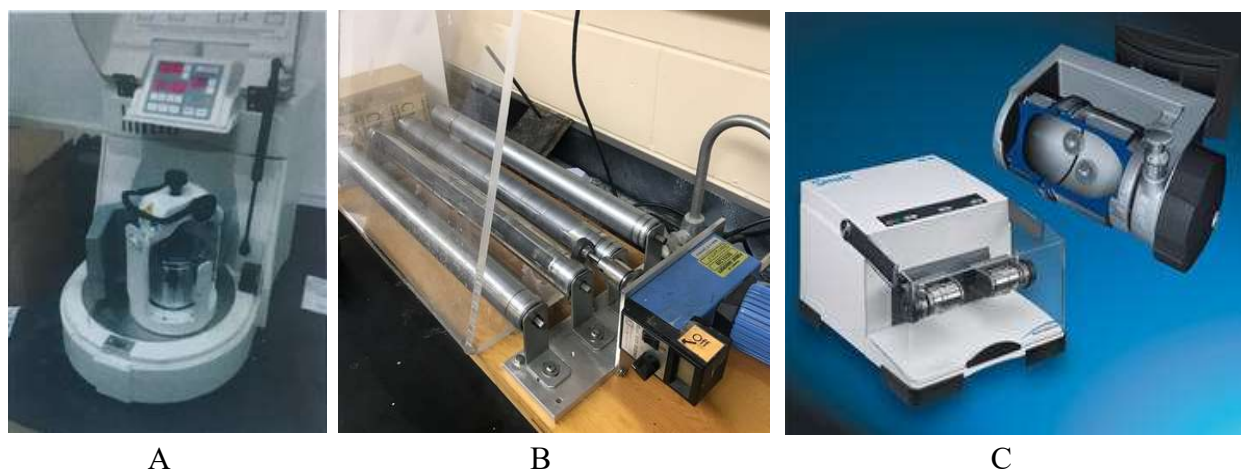


Figure 2.1 Planetary mill (A), Tumbling ball mill (B), and Vibrational mixer (C)

Mechanistic insights into mechanochemical reactions and their distinctions from conventional reactions in solutions are still in its infancy, and most optimizations are obtained empirically. General considerations can be assumed for bond formation, bond cleavage, and catalytic cycles, but mechanistic pathways may diverge for most cross-coupling reactions.⁴⁶ In seminal work conducted in the early 1900s, it was shown that applying mechanical force to silver halide salts resulted in different products than simple heating.⁴⁷ This early observation, now a well-accepted fact, established that mechanochemistry can introduce different reaction pathways that can yield different products *or* product ratios.⁴⁸ In 2015, Friscic et al.⁴⁹ provided compelling evidence using modern equipment and techniques that mechanical activation can give rise to different polymorphs for even archetypal reactions. For example, the reaction between zinc acetate

and 2-methylimidazole normally affords ZIF-8 (a metal–organic framework), but other polymorphs could be formed under specific mechanochemical conditions. Using *in situ* X-ray diffraction,⁵⁰ they showed that a nonporous polymorph (katsenite) could be produced from crystalline ZIF-8 via a fascinating phase change.

Two popular theories arose in the late 1950s that attempted to provide ball-milling reactions with a theoretical backbone that would explain some of the observed phenomena.⁵¹ The plasma model proposed that at the contact points of ball-*to*-ball or ball-*to*-container collisions, a plasmatic surface exists, which provides the heat and unique environment for novel reaction pathways to occur (Figure 2.2B). A more popular and simpler model called the hot-spot theory⁵² proposed that heat at impact collision points is enough for reactions to occur without invoking a plasmatic state (Figure 2.2A).

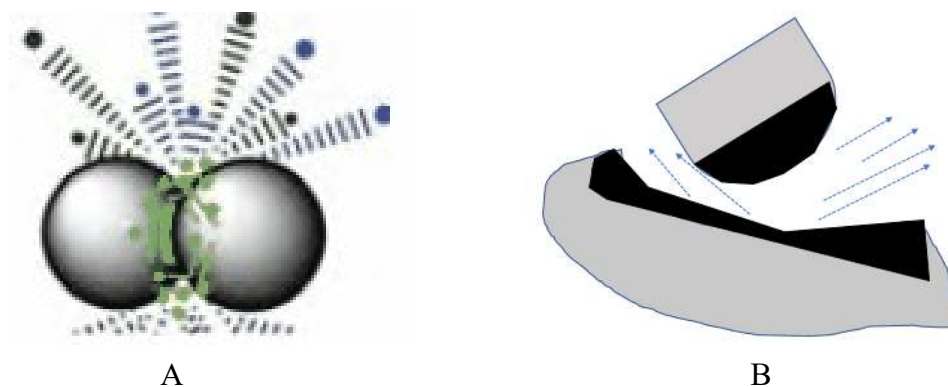


Figure 2.2 Illustrations of (A) hot-spot theory (B) plasma model

The common thread between these theories is that the reactions take place far from equilibrium due to localized heat gradients, which differs from batch reactions in solution where the heat is dissipated evenly throughout the container.⁵³ Stauch and Dreuw published a review that attempts to analyze milling reactions from the perspective of quantum chemistry, in which the effects of physical force on bond formation during collisions are described using molecular orbitals.⁵⁴ In brief, the very act of shearing that occurs causes covalent bonds to bend, which affects the energy levels of the highest occupied molecular orbital (HOMO) and the lowest unoccupied molecular orbital (LUMO). It is the energy gap between these orbitals that determines bond stability.⁵⁵

The high temperatures created at colliding surfaces are generated almost entirely by kinetic energy. Thus, important factors to consider when establishing reaction conditions in mechanochemistry include the type and mass of balls used for milling (Figure 2.3), and the velocity or tumbling rate imparted by the ball mill.



Figure 2.3 Milling media available for mechanochemical grinding

It is important to select the optimal ball size to obtain better yields. Milling balls with relatively low mass or density may not transduce sufficient kinetic energy for bond activation to occur upon collision. On the other hand, if the milling media is too bulky relative to the reaction volume, then their movement within the reaction container is restricted and affects collision rate or velocity. Mack et al.⁵⁶ reported a series of Diels–Alder reactions and compared ball size, milling power, frequency, and container type, which are all important parameters for an efficient mechanochemical reaction. Using a specific type of mill (SPEX 8000M with 13 x 50 mm stainless steel jar), they concluded that the reaction yields changed drastically depending on the media size (18% yield for 4.76 mm balls, versus 8% yield for 6.35 mm balls). Furthermore, the number of balls used during milling could affect yield by as much as 20%. In the same study, they showed that milling in a Teflon container resulted in a lower yield than a stainless-steel container, suggesting a difference in impact energy. The nature of the milling container can also impact the

reaction outcome, namely by the degradation of functional groups by surface impurities or by reaction with the container itself.⁵⁷

The material of the milling media and container (steel, Teflon, zirconium, alumina, and Nalgene, to name a few), the ball size and quantity, and the design of the ball mill itself represent experimental factors that are unique to mechanochemistry. However, extrinsic parameters such as reaction temperature are also important to consider. Collision theory has been employed to explain how reactions occur during mechanochemistry, which merits a more detailed discussion of temperature and activation energy. According to the Arrhenius equation, the number of molecular collisions with the correct orientation, having kinetic energy equal to or greater than the activation energy, increases with temperature. In addition the input frequency of the ball mill should promote molecular collisions and bond activation. Two important questions arise: (1) Can input frequency (which correlates with the number of ball-*to*-ball and ball-*to*-surface impacts) inside a container be correlated with temperature? For example, can conditions be configured so that a ball mill operating at 30 Hz reliably produces an internal temperature of 90° C? (2) What other options are available to control the temperature inside the container?

The answer to the first question is simply No: Temperature is a complex function of milling media and container size and composition, and also the enthalpy of the specific reaction. The only assumption that can be made is that prior to milling, the reagents, container, and media are at room temperature regardless of parameter adjustments. Fortunately, thermometers are available that allows one to monitor and control reaction temperature by adjustment of extrinsic parameters. Emmerling et. al⁵⁸ used *in situ* Raman Spectroscopy with thermography to analyze temperature flux for crystallization reactions, and Halasz⁵⁹ reported temperature recording using variable-temperature synchrotron powder X-ray diffraction to monitor the coordination chemistry between

cadmium chloride and cyanoguanidine. In the former study, reactions were conducted in a Perspex jar (polymethylmethacrylate, PMMA) with two stainless steel balls at 30 or 50 Hz for 25 minutes. The researchers found that a temperature increase occurred ($\Delta T = 5$ K) for the co-crystallization of theobromine and oxalic acid within the first 5 minutes of mixing, and reached a maximum change ($\Delta T = 11.3$ K) after 12 minutes of milling at 30 Hz. Similarly, the co-crystallization of pyrazinamide and oxalic acid at 50 Hz produced a temperature spike after 5 minutes of ball milling with a maximum increase of 36 K after 10 minutes. The distribution of temperature is important in a ball-milling reaction and its effect on product formation.

An insightful study by Mack et al.⁶⁰ describes the general trend seen in mechanochemical reactions in terms of yield and activation energy (kcal/mol). Figure 2.4 describes three regions that constitute a characteristic profile change during a typical milling reaction. In Region I, the initial temperature is produced by the heat of the reaction itself, regardless of milling frequency and mostly independent of collisions between media. Region II is dependent on collision frequency *and* better mixing after a given time, resulting in a more homogenous blend allowing for comparable energy distribution. Region III is at a late stage of the reaction, and is proposed to represent leftover reagents or intermediates that are less reactive under mechanochemical conditions. In conclusion, the greatest contribution to thermal energy in a typical milling reaction due to collisions can be assigned to Region II.

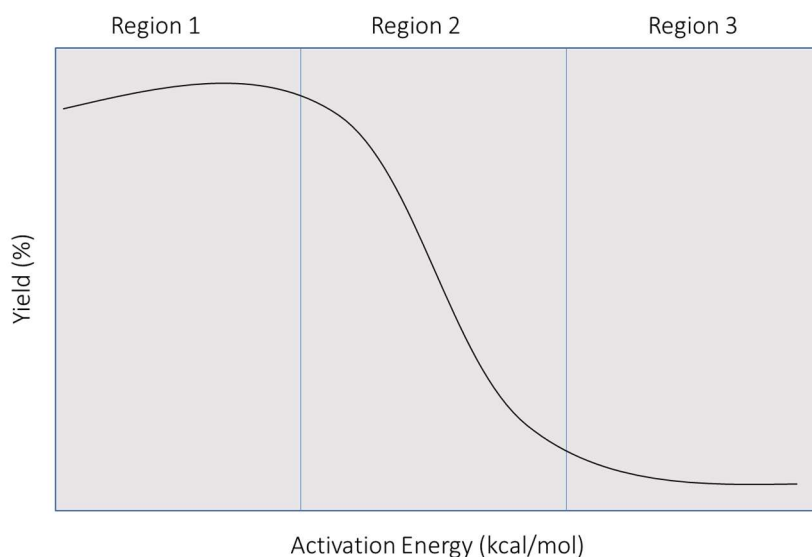


Figure 2.4 General trends of regions during a milling reaction

The methods to control temperature inside the container of a milling reaction are not as convenient as with solution reaction vessels, which can be heated or cooled by an external bath. Reaction mills can be monitored via non-contact thermography, whose temperatures will depend on specific combinations of container type, ball size and number, media composition, and input frequency. In most cases, reports of mechanochemical synthetic methods omit this information with product yield and reaction time being sufficient to prove the success of the method.

2.2 Mechanochemical Grafting of Cellulose Nanofibers and Degree of Substitution Analysis

While the foundations of mechanochemistry are now well established, its application to the chemical modification of cellulose grafting is still relatively novel, although not with precedent. An early account by Hirotsu et al.⁶¹ demonstrated that crystalline cellulose could be grafted onto maleated polyethylene after 24 hours of low speed (horizontal) milling at 250 rpm. The resulting material was melt-processable and showed improved thermal and mechanical properties. The

grafting of small molecules was demonstrated by Huang et al.,^{62,63} in which NC was milled with hexanoyl chloride for 16 hours in a zirconium (Zr) container with 10-mm Zr balls. Although a high degree of substitution (DS) was achieved, considerable amounts of dimethylformamide (DMF) was used (23 mL/0.5 g CNF), which hardly qualifies as LAG. Indeed, the reaction may have worked simply with mechanical stirring. Nonetheless, the resulting film had good optical transparency, indicative of the dispersion quality that was obtained post-modification.

The stable dispersion of surface-modified CNs in an organic solvent is the most definitive test of a successful surface modification; however, DS provides a quantitative measure of *covalent* surface grafting. FT-IR and solid-state ¹³C NMR also provide important spectroscopic characterization for surface-modified NCs, and both methods are applicable to solid-state samples, bypassing the need to prepare stable solutions. FT-IR is especially useful for characterizing the esterification of CNFs: The carbonyl (C=O) stretches between 1600 and 1800 cm⁻¹ serve as the primary indicators of successful surface modification, as pristine (unmodified) CNFs do not produce this absorption band. Two other important regions of the IR spectrum include: (1) absorption peak between 3200–3700 cm⁻¹ that correspond with OH or NH vibrations, and (2) the appearance of C–H stretching modes in the 2950–2850 cm⁻¹ region originating from aliphatic groups (e.g. fatty acids) that have been grafted onto CNF surfaces. In solid-state ¹³C NMR, the majority of signals relevant to cellulose lies with a narrow range (60 to 110 ppm); this simplifies analysis of surface esterification, as the carbonyl peak is easily identified near 170 ppm.

The DS for CNCs has been estimated using elaborate equations, based on the average dimensions of these rod-like structures.⁶⁵ In the case of CNFs, which have variable thickness as well as lengths, methods have applied to determine DS. Elemental analysis is one way to obtain DS values from bulk samples, namely by comparing the mass ratios of C, H, O, and other elements

introduced by grafting. Another simple and popular method is by relative change in mass, as done in the work by Huang et al. using Equation 1,⁶² which has one constant and three variable (m_1 , m_2 , and M_w). The constant is the molar mass of an anhydroglucose unit on the CNF surface (162 g/mol). M_w is the molar mass of the functional group grafted onto the CNF. In the case of the study by Huang et al., a hexanoyl group (98 g/mol) was used. The last two variables, m_1 and m_2 , represent the initial dry mass of CNF and final dry mass of the esterified product post washing and drying, respectively. This simple calculation was also utilized in our own studies.

$$DS = \frac{162 \times (m_2 - m_1)}{M_w \times m_1} \quad (1)$$

Equation 1 DS calculation by weight change before and after surface modification

The third method for estimating DS is based on FT-IR and solid-state ¹³C NMR analysis, with the former utilizing the ratio of peak intensities of the C=O stretch (from the ester group) and C–O stretch near 1050 cm⁻¹. Solid-state NMR methods for calculating DS use the ratio of integrated areas of either the C=O peak to total cellulose carbon signals,⁶⁶ or the terminal methyl group of the grafted aliphatic chain to total carbon signals.⁶⁷ Correlations of DS values obtained from these three methods are often variable, but acceptable as a relative method of comparison.

Complementary to the “green chemistry” developed thus far with biorenewable CNFs and solvent-free mechanochemistry, work by Colacino et al.⁶⁸ showed that formation of reactive carbamate intermediates can be facilitated using 1,1'-carbonyldiimidazole (CDI) under neat conditions (Figure 2.5). CDI is a versatile reagent used to activate carboxylic acids for their addition to alcohols and amines. The byproducts and driving force of the reaction, carbon dioxide and imidazole, are not environmentally hazardous and easily separated from the reaction products. CDI is also relatively cheap (<\$1/kg) and widely available from many vendors. Its use in

mechanochemistry has been demonstrated and shown to be effective in preparing amides, esters, ureas and carbamates in the absence of solvent.⁶⁸ We reasoned that CDI would be a useful reagent for activating fatty acids (e.g. oleic, lauric, and stearic acids) and other low molecular weight carboxylic acids (e.g., benzoic and furoic) for the surface modification of CNFs. Mechanistically, the steps for CDI activation are presumed to be the same as in solution, which was studied in the 1960s for peptide coupling.^{69,70} Carboxyl activation involves the formation of an acyl carbonylimidazole, which decomposes into CO₂ and a metastable acylimidazole. This intermediate then reacts with secondary nucleophiles, such as the primary hydroxyls on the CNF surface.

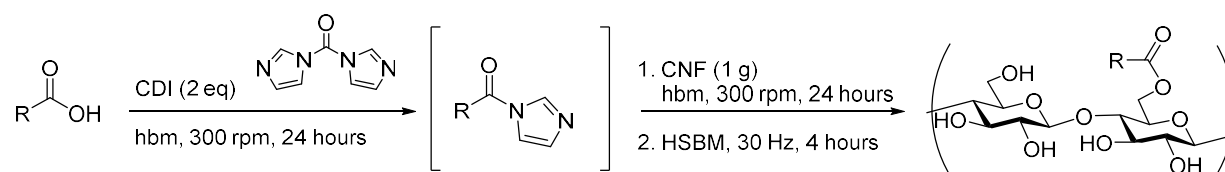


Figure 2.5 CDI-mediated CNF surface functionalization. hbm = horizontal ball milling

The remainder of the chapter will focus on applying the principles discussed thus far into practice, with the key strategy being the design of scalable reactions with a minimal increase in carbon footprint. CDI-mediated esterification of CNFs using various carboxylic acids with high DS values will be described, as well as their impact on the enhanced miscibility of surface-modified CNFs in different solvents.

2.3 Experimental

Instrumentation

^{13}C CP-MAS spectra were obtained for modified and unmodified CNFs using a Chemagnetics CMX-400 NMR spectrometer running SpinSight software and equipped with a wide-bore magnet and a 5-mm triple-resonance (H-X-Y) MAS probe. The “CP_TOSS_PM” pulse sequence was used, which includes the TOSS^{71a} and TPPM^{71b} techniques. Acquisition parameters included ^1H and ^{13}C RF field strengths of 50 KHz, a cross-polarization time of 2 ms, a TPPM decoupling pulse of 8.5 μs , a relaxation delay of 4 seconds, a data acquisition time of 32 ms with a sweep width of 32 KHz, and a sample spinning rate of 5.6 KHz. 2048 scans were acquired for each sample (experiment time of 137 minutes) and the data was processed with exponential weighting (line-broadening of 35 Hz) and zero-filled twice prior to Fourier transform analysis. ATR-IR spectra were obtained in transmission mode for qualitative analysis of modified and unmodified CNF using a Thermo Nicolet Nexus spectrometer equipped with a MCT detector (800–4500 cm^{-1}), KBr beam splitter and Diamond ATR. UV-Vis spectra were obtained using a Varian 50 spectrophotometer. Sonication of CNF suspensions was performed using an UltraSonics Processor with a 13-mm Ti immersion probe at maximum power for intervals of 5 seconds sonication with 10 seconds rest, over a period of 45 minutes.

General Procedures

All starting materials and reagents were obtained from commercial sources and used as received unless otherwise stated. Mass recoveries were calculated instead of yields; values lower than the initial CNF indicated some loss of modified CNF during isolation. DS values were

calculated by using Equation 1 with the appropriate M_w values corresponding to the target grafted molecule.

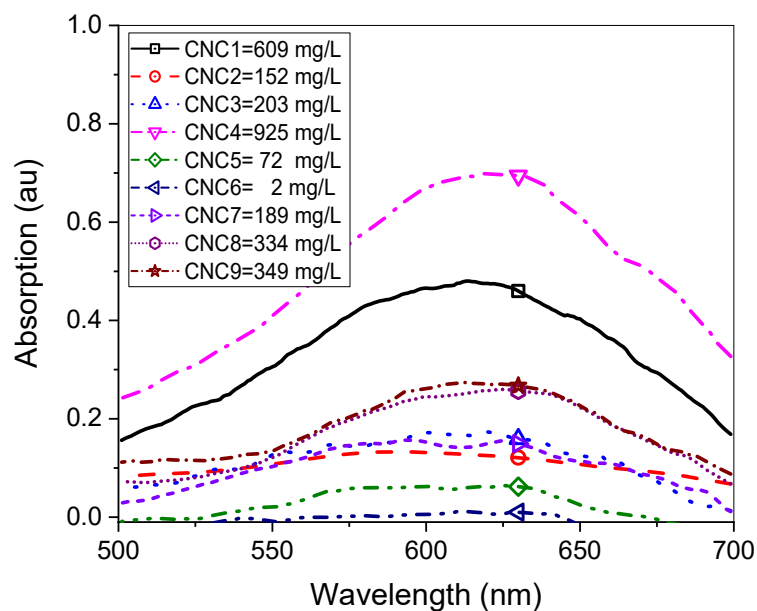
CNFs were obtained from Forest Product Laboratories (University of Maine) as a 3 wt% slurry, with a distribution of widths and lengths of 5–200 nm and 130–225 μm , respectively as provided by the suppliers. Freeze drying was performed on 300-gram aliquots of 3 wt% CNF in plastic containers; these were first frozen overnight at $-20\text{ }^\circ\text{C}$, then lyophilized for 4 days in a Labconco FreeZone Console Freeze Dry System (collector temperature set at $-50\text{ }^\circ\text{C}$).

Covalent modification of cellulose nanofibers was conducted using a homemade low-speed horizontal ball mill, built by the Jonathan Amy Facility for Chemical Instrumentation. The freeze-dried cellulose nanofibers were granulated with a coffee grinder prior to ball milling. Carboxylic acid and CDI were combined in a 120 mL NALGENE bottle equipped with ten Zr balls (9 mm) and milled for 24 hours. The bottle was vented carefully to release any CO_2 , followed by the addition of 1 g freeze-dried CNF and milling for an additional 24 hours. The resulting white powder was then transferred into a 500-mL Erlenmeyer flask, suspended in an aqueous solution, and stirred for 30 minutes. The modified CNFs were filtered to produce an off white powder which was dried in air for 1 hour, then kept under vacuum overnight to ensure the removal of all volatiles.

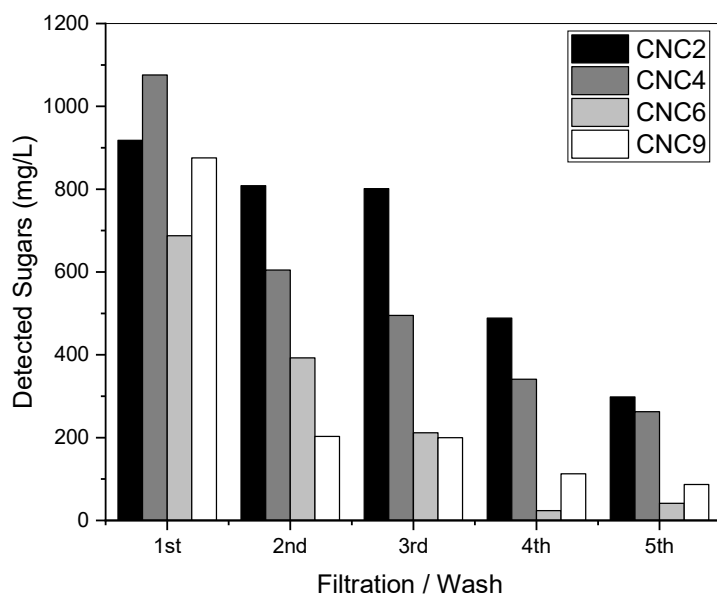
2.4 Results and Discussion

CNCs were originally considered as a viable starting material for mechanochemical esterification, but chemical analysis (anthrone assays) showed varying amounts of free sugars in different commercial sources of CNCs (Figure 2.6A). Under acidic conditions, anthrone reacts with furfuryl aldehydes (the decomposition product of free sugars) to yield species that are detectable at 630 nm by UV spectroscopy. Attempts to wash CNCs by ultrafiltration showed a

gradual decrease in the amount of detectable free sugars, but substantial amounts remained even after five tedious washes (Figure 2.6B).



A



B

Figure 2.6 (A) Free sugar concentration detected for various samples (B) Wash cycles and detected sugar amounts

Nevertheless, CNCs were used in our early ball-milling studies, using bases such as imidazole and K_2CO_3 as well as liquid-assisted grinding with DMSO. Carboxylic acid derivatives included dodecyl succinic anhydride, lauryl and stearyl chloride, and oleic acid activated with CDI. Ball-milling reactions could be run on a 50-gram scale, which was successfully demonstrated for stearylated CNCs.

CNFs were favored over CNCs because of their low free sugar content and reduced chemical processing. Namely, CNFs do not require harsh acid for digestion, which makes them even more eco-friendly than CNCs. We first investigated several different methods for drying aqueous CNF slurries into processable powders (see Chapter 3 for method evolution), and used a planetary ball mill (FRITSCH PULVERISETTE 6 classic line) for mechanochemistry. However, CDI-mediated stearylolation of dried CNFs gave mixed results, with most reactions containing degradation byproducts from the heat generated. Although variations in MC conditions yielded some improvement, reproducibility was limited (Table 2.1 and Figure 2.7).

Table 2.1 Some early mechanochemical conditions

Entry	Instrument	Result
1	Planetary pulverizer (colloidal CNF), 400 rpm	Success (but hard to repeat)
2	Horizontal Ball mill (fluffy CNF, 400 rpm)	No reaction
3	Planetary Pulverizer (fluffy CNF), 400 rpm	No reaction
4	Horizontal Ball mill (fluffy CNF, 550 rpm)	Success



Figure 2.7 MC conditions using a planetary ball mill. Significant degradation or charring of reaction materials was observed.

The use of a high-speed ball mill (MSK-SFM-3, MTI Corp.) with lower input energy gave better results and also allowed us to systematically vary the MC reaction conditions. Reaction parameters (ball and container type) were optimized empirically at a frequency of 30 Hz; the relative efficiency was measured by calculation of DS values of the products from freeze-dried CNFs and stearic acid activated by CDI (Table 2.2). Esterified CNFs were purified by transferring the dry reaction mixture to a 150-mL Erlenmeyer flask, adding 100 mL EtOH, and stirring for 30

minutes. The solution was then poured into a Buchner funnel and washed twice with additional EtOH. The filtered solid was dried in air, and then overnight under vacuum.

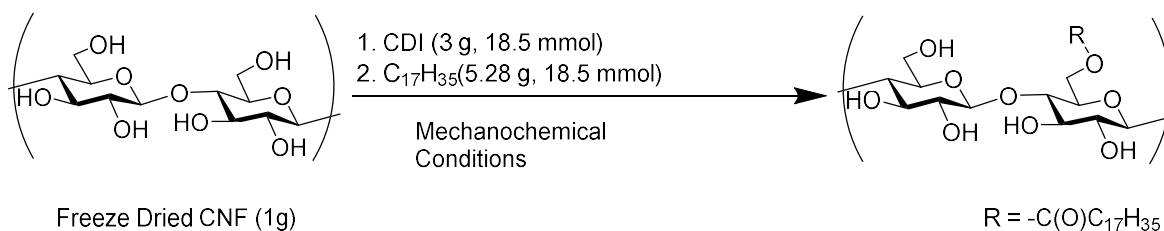


Table 2.2 Optimization of conditions using high-speed ball mill (Zr = Zirconium balls, SS = stainless steel, Alum. = alumina)

ID	Ball Type	Container	Time	Hertz	DS
1	Zr	Nylon	60 min	25–30	0.05
2	Zr	SS	60 min	25–30	0.1
3	SS	SS	60 min	25–30	(neg. value)
4	Alum.	SS	60 min	25–30	0.08
5	Alum.	Nylon	60 min	25–30	0.06
6	Zr	SS	240 min	25–30	0.18

The reaction times shown in Table 2.2 (entries 1–5) were kept constant for quick evaluation. Extending the milling time from 12 to 24 hours greatly improved DS values to as high as 0.9, whereas a milling time of 6 hours or less was insufficient. The sequential addition of reagents was also found to be crucial. A separate study had been conducted in which the CNF was added with CDI and stearic acid in one pot, versus activation of steric acid with CDI and subsequent addition of CNF. The former gave a DS of 0.7 after 24 hours milling, whereas the latter gave a DS close to

1.0. The combination of stainless steel balls and container resulted in discoloration, suggesting that these materials were deleterious to the reaction. On the other end, Zr or alumina balls with nylon containers gave lower DS, which can be attributed to material “softness” of the nylon container, and lower collision energy. However, reproducibility remained an issue, and reactions in the high-speed ball mill were limited in scale (an important consideration for this research project).

We then performed MC reactions using a horizontal ball mill operating at low speeds (30–35 rpm), which could support up to 18 reaction vessels at once (Figure 2.8). Horizontal ball milling was performed using Zr balls in NALGENE bottles, which are cheap and available in many sizes. This condition yielded grafted CNFs with respectable DS values (Table 2.3); IR spectroscopy revealed a strong characteristic C=O stretch for esters, provided further evidence of efficient grafting (Figure 2.9). Products from successful grafting reactions exhibit a 10–15 cm^{-1} increase in frequency.



Figure 2.8 Horizontal ball milling with Zr balls in NALGENE bottles (30 rpm)

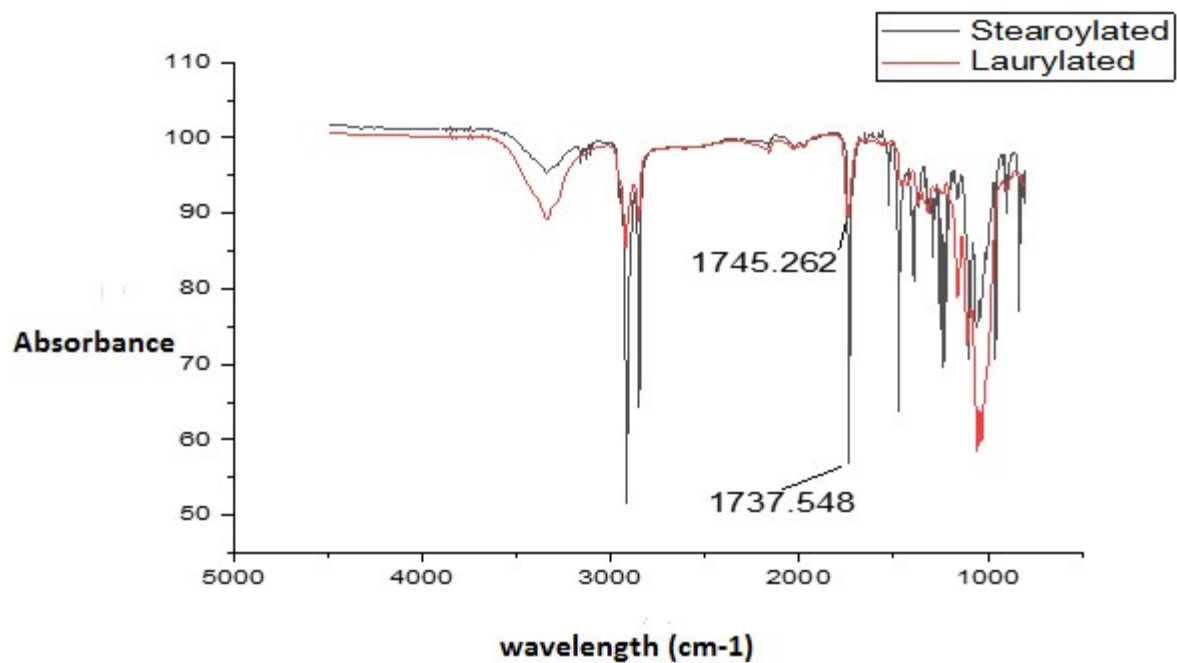


Figure 2.9 IR spectra of CNFs esterified with lauric (C12) and stearic (C18) acid after low-speed milling

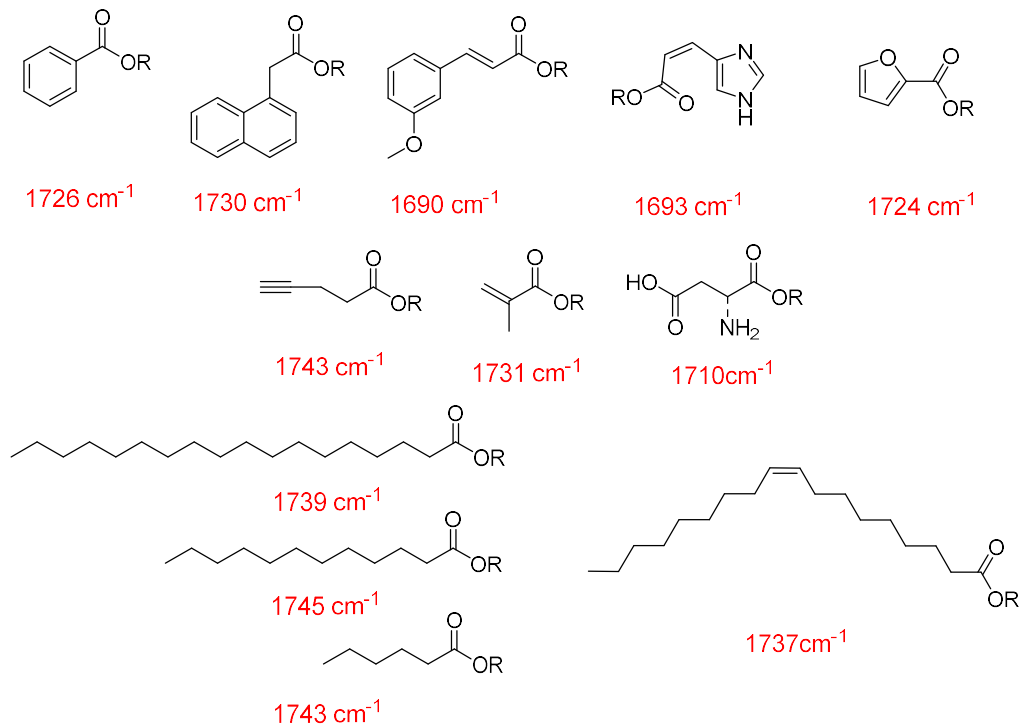


Figure 2.10 Scope of compounds grafted onto CNFs under mechanochemical conditions, with carbonyl ester stretches.

The scope of the horizontal ball milling reaction was extended to other carboxylic acids with various functional groups; IR carbonyl stretches of the esterified CNF products are shown in Figure 2.10. The washing protocol was optimized for each product, by reducing the amount of alcohol or substituting with water whenever possible (Table 2.3).

Table 2.3 DS values obtained and volume and ratio of washing solvents used for various compounds

CNF (g)	CDI (g)	Ester type	RCO ₂ H (g)	Wash (mL/g)	DS (repeat)*
1	2	Propionate (C3)	1.0	Water (10 mL)	0.85
1	2	Hexanoate (C6)	1.4	Water (150 mL)	0.10
1	2	Laurate (C12)	2.5	EtOH:Water (50:160)	0.72
1	2	Stearate (C18)	3.5	EtOH:Water (20:65)	1.36
1	2	Oleate (C18)	3.5	EtOH:Water (70:200)	0.04
1	2	Benzoate	1.5	Water (272 mL, 55 °C)	0.90
1	2	Pyroglutamate	1.6	Water (25 mL)	0.073
1	2	Urocanate	1.7	Water (1140 mL)	0.015
1	2	2-Furoate	1.4	Water (55 mL)	0.48
1	2	Methacrylate	1.06	Water (11 mL)	0.16
1	2	4-Pentynoate	1.2	Water (100 mL)	0.95

*DS = Degree of substitution (esters per AGU)

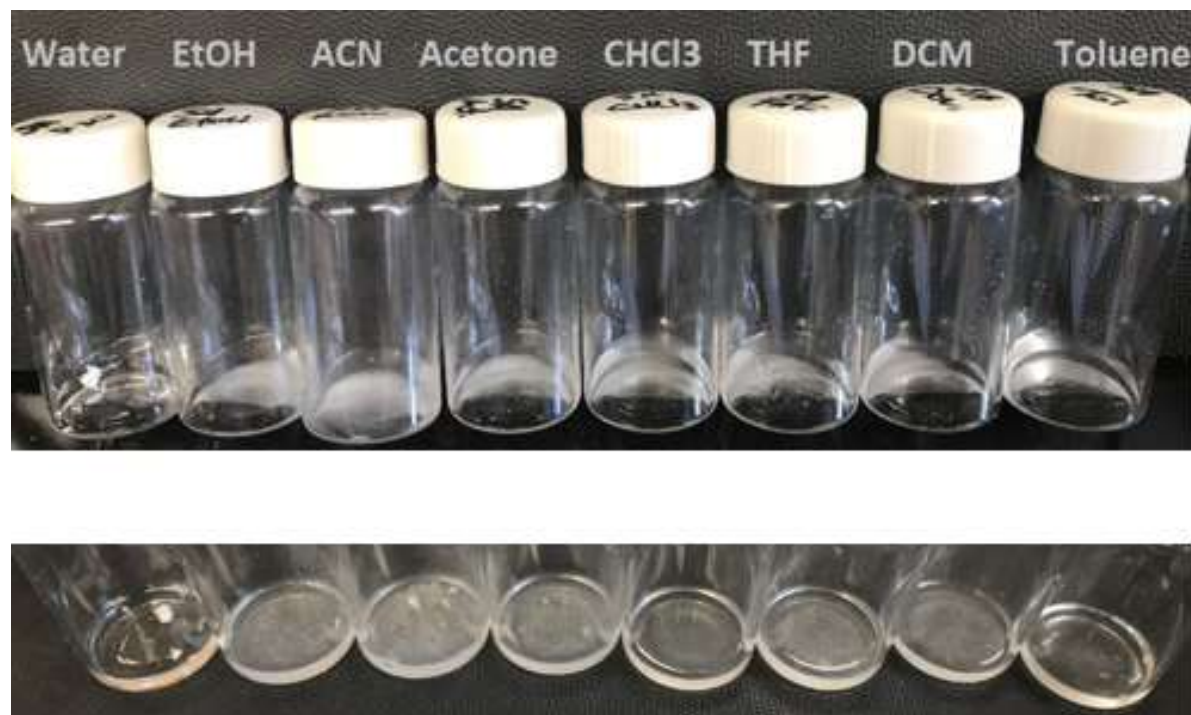
There was no discernable pattern correlating DS to chain length, polarity or any other chemical factor. One probable explanation is that the physical process of milling is more important than steric or electronic factors. For example, stearic acid is a powder that disperses evenly around the milling container upon grinding, whereas oleic acid is sticky and vicious and frequently causes the balls to stick against the walls of the reaction chamber or themselves (Figure 2.11). Propionic and caproic acids are liquids but with low viscosity; although the DS for caproyl-CNF is low the DS of propionyl-CNF is higher possibly due to its smaller molecular size. Overall, the scope of

this solventless grafting method demonstrates that a myriad of functionalized CNFs can be prepared, using only water or aqueous alcohol for washing.



Figure 2.11 Examples of coated balls that arise for vicious starting materials

Having established a reliable MC method of grafting various carboxylic acids onto CNF surfaces, we tested the dispersibility of C18-CNFs and furoyl-CNFs in various solvents. A stable dispersion provides the true mark of a successful CNF functionalization, as it can enable a broad scope of applications based on homogenous blends of materials that can be cast into nanocomposites or thin films. The dispersion behavior of stearylated and furoylated CNF is shown in Figure 2.12.



A



B

Figure 2.12 Functionalized CNF at 1 w/v% concentration in various solvents (A) Stearoylated CNF; (B) Furoylated CNF

Qualitatively, 1 wt% C18-CNFs produced more homogenous dispersions in organic solvents than 1 wt% furoyl-CNFs. This is expected, as the longer chain length of stearic acid should reduce aggregation (steric repulsion) and the energy of solvation in aprotic solvents. However, even in the best cases, the colloidal stability of the functionalized CNFs was poor and sedimented in less than 24 hours.

Fortunately, subsequent studies using CNFs lyophilized with a co-solvent (*t*-BuOH, or TBA) produced surface-modified CNFs with much better dispersion stability in organic solvents (to be discussed fully in Chapter 3). An example is provided in Figure 2.13, in which CNFs modified with various fatty acid derivatives remain stably suspended *after 24 hours*. In comparison, esterified CNFs prepared from freeze-dried samples without TBA dispersed poorly in organic solvents, and were observed to sediment only a few minutes after sonication.

2.5 Conclusion

The mechanochemistry developed for grafting CNFs with carboxylic acids provides a sustainable and scalable method of modifying nanocellulose fibrils in a solvent-free manner. Furthermore, the washing steps were designed to use the minimum amount of ethanol. Systematic evaluation of experimental parameters such as type and number of balls, media container, and milling speed and energy enabled us to optimize conditions for a successful reaction. Further improvements will be discussed in Chapter 3, in which the use of TBA as a co-solvent during lyophilization resulted in CNFs that are more readily dispersible in both modified and unmodified forms, and with subsequently greater colloidal stability.

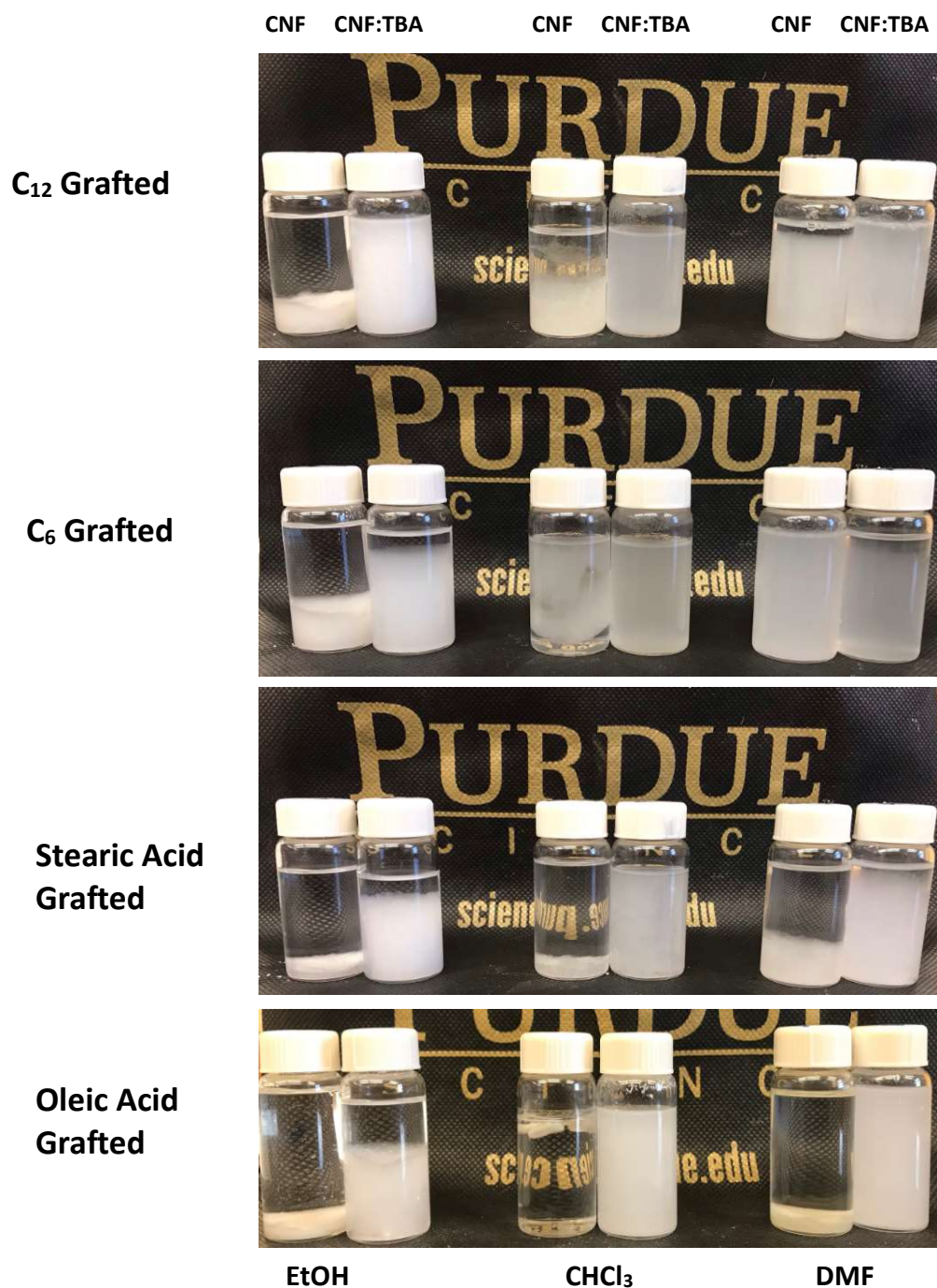


Figure 2.13 Surface-modified CNFs dispersed in various solvents, after 24 hours. Vials on the left were prepared using standard freeze-dried CNFs; Vials on the right were prepared using CNFs freeze-dried from aqueous TBA solutions.

CHAPTER 3. THE ROLE OF CO-SOLVENT IN THE LYOPHILIZATION OF CELLULOSE NANOFIBERS

3.1 Introduction to different drying techniques for CNFs

The two main methods of obtaining CNF from cellulose microfibrils involve chemical treatment and mechanical processing. Regardless of method, the final product is typically a slurry of cellulose nanofibers suspended in water. This aqueous medium allows the native CNFs to remain dispersed, but at the cost of shipping viscous liquids that are least 90% water by weight.⁷² Although many products can be made using cellulose in slurry form, the aqueous mixture prohibits the use of numerous organic reactions that cannot be performed in water. Thus, endeavors to *dewater* CNF pulp have led to a myriad of useful techniques for drying CNFs without destroying their nanoscale architecture.^{73,74} Furthermore, dried CNFs may be useful in composite manufacturing, in which neat solids are processed by melt extrusion blending.⁷⁵

CNF slurries are gelatinous and comprised of an extended network of entangled fibers. However, drying often results in irreversible fiber aggregation and the loss of surface area, a process termed hornification (Figure 3.1).⁷⁶ Essentially, individual nanofibers close distance and form strongly associated, hydrogen-bonded bundles that reduce exposed surface area and resist re-solvation.⁷⁷ It has been shown that hornification increases the tensile strength of paper in direct proportion to increased fiber intercalation.⁸⁶ However, it also causes three detrimental effects in applications where homogenous polymer blends are a prerequisite: (1) more energy is needed to redisperse or untangle the bundled CNF fibers, (2) the agglomerated fibers are unevenly dispersed throughout the matrix, which compromises the intended materials properties of the final nanocomposite, and (3) the decreased surface area reduces the availability of peripheral hydroxyl groups to chemical modification.

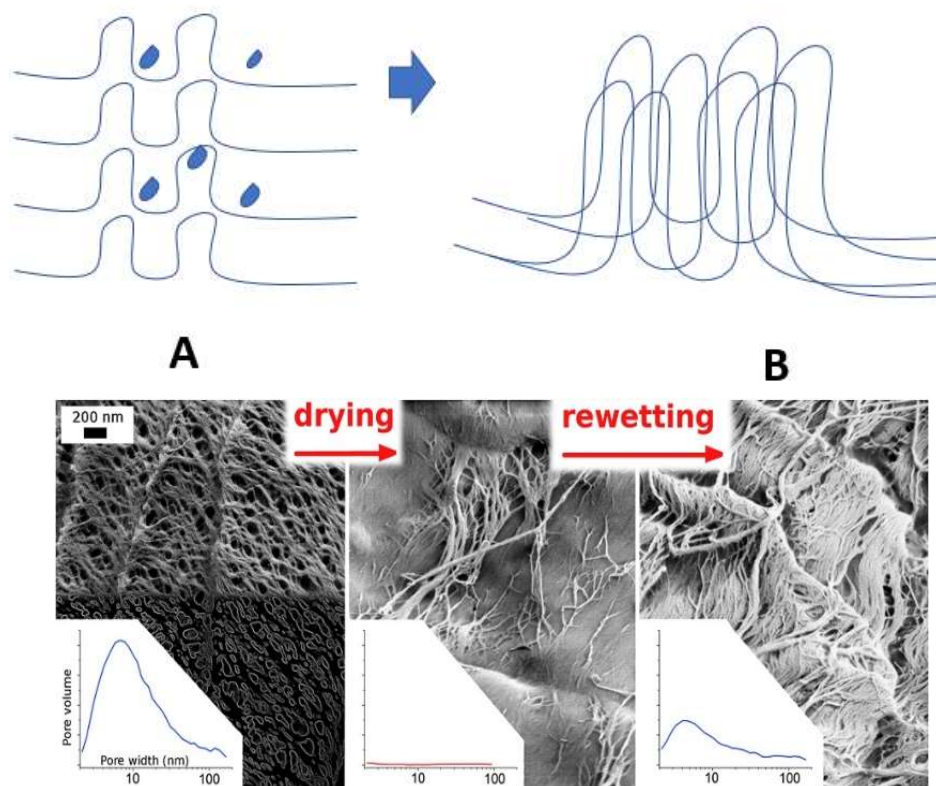


Figure 3.1 (A) Hornification is the irreversible collapse of CNF fibers during the drying process (B) Fiber bundling and pore size reduction as the result of hornification⁷⁷

The four main methods of drying CNFs that have been used extensively are: (1) supercritical drying (SCD),⁷⁸ (2) spray drying (SD),⁷⁹ (3) oven drying (OD),⁸⁰ and (4) freeze drying (FD).⁸¹ The first three methods will be briefly reviewed, followed by a more in-depth discussion on freeze drying (also termed lyophilization or cryodesiccation), the method of choice in our study.

Typically, as water is removed from the surfaces of a suspended network of particles or fibers, capillary forces pull these objects together resulting in a collapsed structure. In SCD, the aqueous medium is displaced by supercritical CO₂, which is nontoxic and relatively inert.⁸² This substitution occurs at high pressure and slightly elevated temperatures. Switching water to a less polar medium reduces the effects that result in hornification, as the high surface tension of the air–

water interface is avoided. However, the instrument and conditions needed to maintain the temperature and pressure above the critical point can be costly.

SD is more common than SCD, and the equipment allows for greater control of experimental parameters. The technique involves dispersing CNF as small droplets, whose increased curvature and lower surface tension accelerate the rate of evaporation.⁸³ Agglomeration of the deposited CNFs is reduced simply because smaller droplets can only contain so much material. However, more research is needed to improve the uniformity of droplet sizes, which is a limitation when the SD process is practiced on an industrial scale.⁸⁴

OD is easily scalable, and conventional ovens are cheap, programmable and user-friendly. However, the direct drying of cellulose nanofibers will surely result in hornification with subsequent loss of nanostructure. The effects of oven drying are similar to that of drying CNF networks under ambient conditions (e.g., gradual evaporation from a CNF slurry in a Petri dish). The slow evaporation of water from a colloidal CNF suspension allows the fibers time to migrate toward each other to create larger bundles, often with dimensions exceeding the nanoscale.⁸⁵ The increased rate of drying in an oven is not fast enough to overcome hornification.

FD, unlike SCD, involved sublimation (a phase change from solid to liquid) under reduced pressure and at low temperatures (Figure 3.2).⁸⁷ Naturally, the CNF slurry needs to be in solid form, which is usually accomplished either by freezing the sample prior to lyophilization or by programming the FD apparatus to perform freezing by a defined protocol. In the latter case, it is recommended that the initial shelf temperature be well below 0 °C to ensure that all the water remains frozen during sublimation, and to enable a smooth phase change below the triple point at which all three phases exist.⁸⁸ For pure water, the triple point is achieved at 0.01 °C and 4.58 mm of Hg.⁸⁹

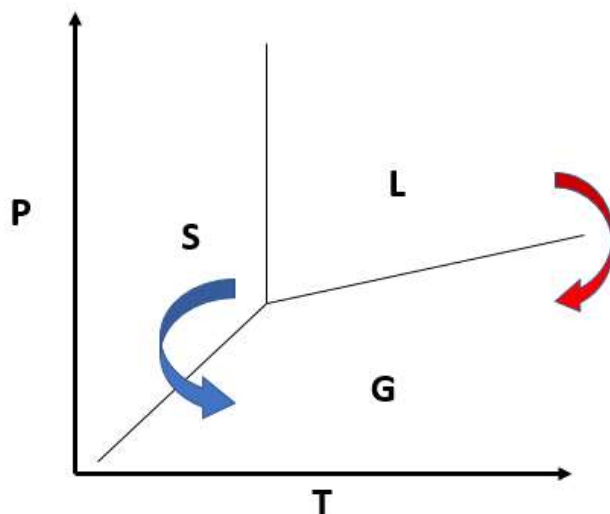


Figure 3.2 Diagram of the phase changes involved in FD (blue arrow) and SCD (red arrow)

Initially, the frozen samples are in a low-pressure environment at the highest temperature possible, although usually still below the triple point. The reason for the higher temperature during this primary drying stage is that it allows for the rapid sublimation of over 90% of the water onto the condenser. Care should be taken to balance the rate of sublimation with changes in temperature, as large variations in heat can induce cake collapse and compromise the quality of the freeze-dried material. Secondary drying, the last step prior to obtaining the fully dried product, involves the desorption of any remaining water strongly bound to the solute (i.e., water associated with surface hydroxyls on CNFs). Many FD systems are programmed to elevate the shelf temperature at this stage, to accelerate water desorption at the ice–solute interface. However, this should again be performed with care, as rapid desorption can also draw adjacent fibers together to cause irreversible cohesion and entanglement.

The eutectic point of the solid sample is an important factor in the FD process that affects many parameters prior to and during sublimation. The eutectic temperature (T_E) is defined as the

freezing point for a specific composition (solute wt%), and is always lower than the freezing point of any single constituent.⁹⁰ A prerequisite for effective FD is to maintain the sample in solid form throughout the process, so it is vital that the temperature remains below the T_E of the frozen mixture. This is also referred to as the critical formulation temperature (CFT),⁹¹ and is synonymous with T_E for crystalline materials and T_g for amorphous samples. In either case, performing FD above the CFT can result in cake collapse or meltback, which is qualitatively observed when the shape of the FD product is deformed relative to its container.

The use of FD as a method to convert CNF emulsions into solid-state forms without loss of porosity has been reviewed previously, especially as a method of forming aerogels.^{81,92,93} Cellulose fibers can be reorganized during ice crystallization, which affects their 3D network structure in its final freeze-dried state as characterized by SEM. High-aspect ratio ice crystals often grow in a direction dictated by the CNF fiber axes; in turn, the ice crystals create a perimeter encouraging unidirectional fiber alignment.⁹⁴ If the fibers are closely packed, they can collapse into micron-sized bundles and multi-lamellar sheets (i.e. hornification). On the other hand, if the fibers are initially well dispersed, the CNF network after primary drying should be highly porous and comprised mostly of fibrils with diameters below 100 nm, so it is important to identify FD conditions that can preserve these nano-architectural features. In the next section, we discuss strategies to prevent structural collapse of the CNF network during FD, using insights gleaned from pharmaceutical process research.

3.2 Cake Formation/TBA: Importance and Interpretation

Lyophilization of pharmaceutical drugs into a solid matrix increases their stability and shelf life, relative to liquid formulations.⁹⁵ Mild heating is used to drive sublimation below the CFT,

which also preserves the active pharmaceutical ingredient (API). FD is thus categorized as a “soft” drug processing technique. Extensive studies and reviews have been published on FD methods for preserving API in commercial drug formulations.⁹⁶ The focus of this section will be on the qualitative analysis of FD products in the form of cakes and on the use of co-solvents to improve conditions during lyophilization. This type of data is important, as cake morphology is a strong indicator of successful FD and API stability. In the case of CNFs, the quality of cake formation can be translated into the final morphology of the fiber network, which dictates subsequent dispersion and colloidal stability. In other words, poor cake appearance is often correlated with poor dispersion.

One good way to assess cake quality is whether the FD product retains the same volume and shape as its container prior to freezing. Various deviations from ideal (elegant) cake formation are described with colorful labels such as collapse, meltback, puffing, slanting, lifting, cracking, shrinkage, coloring, and dropping (Figure 3.3).⁹⁷ A detailed description of each deformation is beyond the scope of this chapter, but some general guidelines will be helpful to appreciate their occurrence in CNF cake formation.

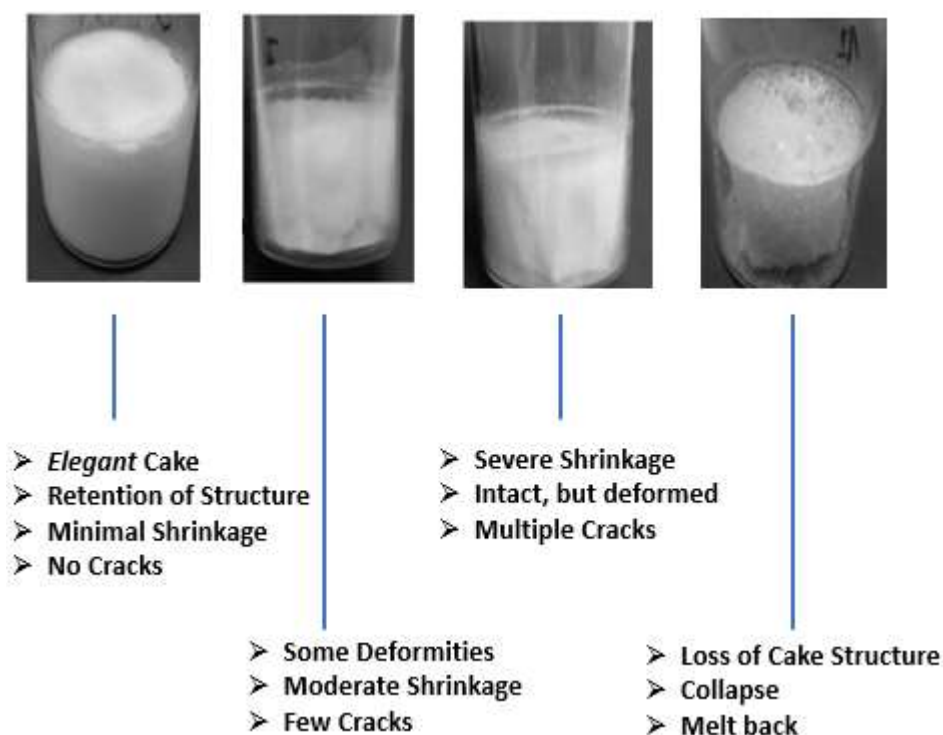


Figure 3.3 Cake appearance as an indicator of freeze-drying quality.⁹⁷

Regardless of deformation type, all non-ideal cakes share two common assumptions: (1) there are no strict references of what is acceptable, rather the results are analyzed based on empirical precedent (i.e. a historical database of earlier cases), and (2) deformation is a strong sign of poor long-term stability, although there is a margin of tolerability. Often, a freeze-dried product can experience shrinkage or collapse but still be useful. Due to the energy cost of FD processes imperfect batches are not thrown out, but each sample is analyzed individually which is a laborious and time-consuming process.⁹⁸

Cake collapse is the result of defective microstructures that are often produced when CFT is surpassed, allowing a liquid phase to form inside the matrix with subsequent loss of physical structure. Often the result is not so much perimeter shrinkage, but a visible downward collapse of the top layer. Furthermore, the liquid phase can re-solidify followed by sublimation that leaves

amorphous drops termed meltbacks. Finally, two important terms that need to be addressed are shrinkage and cracking. Shrinkage is tested simply by inverting the container and allowing the solid to fall out, whereas cracking is quickly identified by visible crevices and canyons on the top or side of the dried cake. In the pharmaceutical industry shrinkage and cracking do not *necessarily* mean poor API stability, but simply indicate the poor mechanical integrity of the matrix.⁹⁷ However, in our CNF studies their appearance correlated with hornification of varying degrees. This implies that the agglomeration of fibers result in overall decrease of cake height and width upon sublimation.

Co-solvent systems in which water is diluted with an organic solvent have been shown to help not just with cake stability, but also many other practical aspects such as solubility and a reduced FD processing time.⁹⁹ Disadvantages of such systems include the low flash point of organic solvents, the increased cost of disposing solvent waste, and added precautions to ensure that no impurities or byproducts are generated in the final product.¹⁰⁰ Compatible solvents for FD with aqueous suspensions include, but are not limited to, *tert*- and *n*-butanol (TBA and NBA), ethyl acetate, ethanol, acetonitrile, acetone, and methanol.¹⁰¹

The role of co-solvents has been studied extensively.^{99,100,102,103} By almost all accounts the effect of binary solvent systems begins with freezing. In our study, the organic solvent used was TBA, which is fully miscible in water and forms well-defined eutectic mixtures. For example, the T_E is $-5\text{ }^\circ\text{C}$ for a 20 wt% TBA solution, and $-3\text{ }^\circ\text{C}$ for a 90% solution.¹⁰⁴ Akira et al. demonstrated the use of 40% TBA in the lyophilization of TEMPO-oxidized cellulose nanofibrils (TOCN) to produce aerogels surface areas greater than $300\text{ m}^2/\text{g}$, compared to untreated TOCN with a surface area of $100\text{ m}^2/\text{g}$.⁸¹ However, a decrease in surface area was observed when 1:1 water:TBA (v/v%) was used, indicative of TOCN aggregation during lyophilization. The authors also observed a more

uniform distribution of TOCN fibers by SEM imaging. Laminar sheets were clearly visible in untreated TOCN samples versus samples lyophilized from 10% to 50% TBA, whereas the author surmised that the lower eutectic point of water–TBA mixtures reduced the size of ice crystals during freezing below micron dimensions.¹⁰⁴ Dongyeop et al.¹⁰⁵ also showed that dispersions of oven-dried CNC and CNF can be modulated by adding TBA to aqueous emulsions prior to heating, although surface area data was omitted. The authors suggested that the lower surface tension of water–TBA mixtures helps limit the “dragging” effect as explained previously.

The objective of this chapter is to study the use of a lyophilization co-solvent such as TBA on the dispersibility of CNFs post-lyophilization, using cake integrity as a visual predictor of positive effects. Absence of shrinkage, meltback and cake collapse were also positive indicators that a suitable mixture of TBA and aqueous CNF slurry had been achieved.

3.3 Experimental

A Labconco freeze dryer with shelves (FreeZone Bulk Tray 77530) was used in all lyophilization studies. In a typical experiment, a 100-mL polyethylene container with 3% aqueous CNF slurry (80 g) and TBA (20 g) was placed in a –20 °C freezer overnight covered by a tissue paper. The collector was precooled to –50 °C prior to placing the frozen sample on the vacuum chamber shelf, which was kept at room temperature (20–23 °C). Lyophilization was conducted at .092 torr over a period of 4 days without controlling the shelf temperature.

In a typical procedure to functionalize lyophilized CNFs (TBA treated) the cake was first broken up into smaller pieces so as to fit inside the coffee grinder. Then the grinder was turned and stopped only after all the cake had been made into a fluffy like solid. In a NALGENE container (200 mL) equipped with 11 Zr balls was added oleic acid (1 g) and CDI (2 g) and milled for 12 hours with opening of the cap after 1 hour to release CO₂. Then the grinded CNF/TBA solid was

added to the container, mixed in with a spatula and milled for an addition 12 hours. Finally, the mixture was deposited into a 500 mL Erlenmeyer flask and washed with EtOH (100 mL) or EtOH: H₂O (70: 200 mL) mixture. Filtration of the solution by way of Buchner funnel with a Whatman filter paper followed by 5x wash with EtOH or EtOH: H₂O mixture yield a thick film. The film was allowed to air dry overnight or can be dried via vacuum. 200 mg of the dried OA-CNF was added to a beaker along with 20 mL of CHCl₃ and probe sonicated for 45 minutes at maximum power (5 seconds ON and 10 seconds OFF) to yield the dispersed solution.

3.4 Results and Discussion

The conversion of CNF slurries into processable solids was pursued with two goals in mind: (1) to achieve a dehydrated state within a short time, and (2) to obtain a fine powder with high surface area for subsequent mechanochemical functionalization. Initial attempts at oven drying of undiluted CNF slurries resulted in hardened blocks that were unworkable; the hardness of the dried CNFs made it almost impossible to grind them into finer powders for MC modification. Treatment of CNFs with several washes of acetone was found to be effective at dewatering CNF slurries by simple filtration and drying at room temperature, with the final dry mass stabilizing at 3.1 wt% of the initial wet mass after four days (Figure 3.4 and Table 3.1).



Figure 3.4 Dewatering of acetone-treated CNFs resulted in hardened flakes that resisted further processing

Day	Mass (g)	Relative Mass%
1	16.1	17 %
2	3.27	3.5 %
3	3.16	3.4 %
4	3.10	3.3 %

Table 3.1 Relative mass changes of air-dried CNF samples after dewatering with five acetone washes (initial wet mass = 94 g)

Significant volume shrinkage, a qualitative indicator of hornification, was observed for the acetone-washed CNF samples after only one day of air drying inside a Petri dish (Figure 3.5). Oven heating of the acetone-washed samples exacerbated deformation from a planar form (curling at the edges), and produced a hardened disk that resisted further processing.



Figure 3.5 Shrinkage and curling of air- and oven-dried CNFs, dewatered by acetone washing

Various pressing methods were tested to improve drying, such as using a mechanical load during heating or vacuum drying (Figure 3.6). This helped to keep samples from warping and also reduced the drying time, but resulted in a stiff, hardened solid that could not be broken into finer granules for ball milling. We also investigated the drying effects of different co-solvents to determine whether pressed CNFs could be dried to completion more rapidly without significant hardening. Polar solvents such as methanol, ethanol, isopropanol and ethyl acetate were tested, however in all cases shrinkage and hardening occurred to such an extent that we abandoned this the approach.



Figure 3.6 Vacuum drying of dewatered CNF samples under a mechanical load

We then evaluated lyophilization as the primary dewatering method. FD of frozen CNF slurries took up to four days for complete desiccation. As expected, interrupting the FD process prior to complete desiccation had an adverse effect on samples that were allowed to warm at room temperature. If the sample was not fully freeze-dried, the gradual evaporation of residual water at ambient temperature and pressure would result in hornification and deformation of the CNF cake (Figure 3.7, *left*). For example, CNF samples that were freeze-dried for 48 hours and left to dry at room temperature formed a porous and hardened material (Figure 3.7, *right*).



Figure 3.7 *Left*, lyophilized CNF samples taken out at different time periods (1–4 days). *Right*, porous and hardened CNF cake after partial lyophilization then drying under ambient conditions.

Completion of FD over the full 4-day period afforded the best quality CNF cakes, which were stiff but still sufficiently malleable to be ground into powder. We initially used a hand-operated kitchen grinder with two different coarseness grades for shredding bulk CNF (Figure 3.8). However, the CNF grains did not break down during MC ball milling, and their interiors remained inaccessible to chemical modification. We then used an electric coffee grinder to reduce the CNF particles to finer grain sizes for subsequent mechanochemistry. The ground FD-CNF particles were considerably more amenable to MC, compared to those produced by simple air drying.

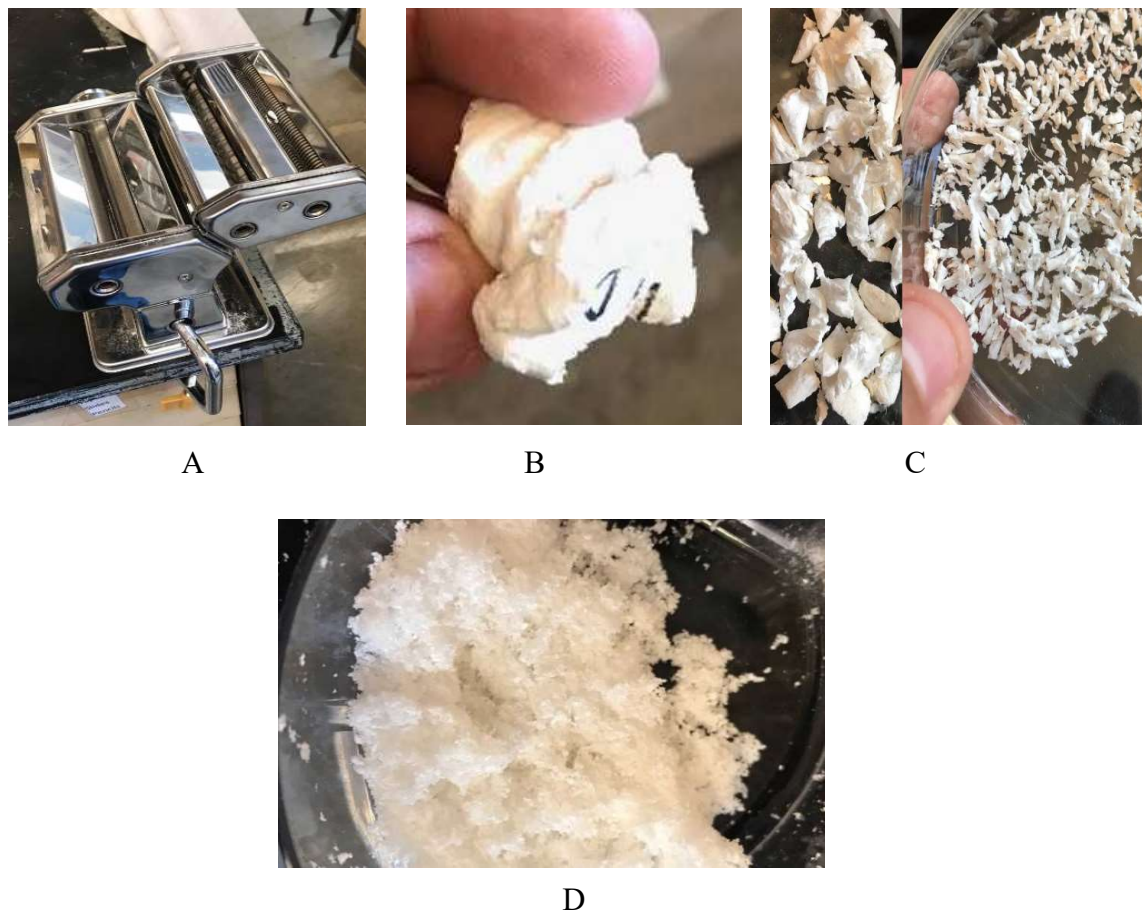


Figure 3.8 (A) Benchtop (manual) kitchen grinder used to shred freeze-dried CNF into coarse grains; (B) Freeze-dried CNF before grinding; (C) CNFs after being subjected to coarse and fine shredding by manual grinder; (D) Further reduction of CNF grains using electric coffee grinder

The cake appearance of the FD-CNFs showed both collapse and shrinkage, even if left undisturbed during the 4-day sublimation window (Figure 3.9, *left*). In addition, the colloidal stability of the redispersed FD-CNFs in water was poor, as characterized by its rapid sedimentation (Figure 3.10, *right*).

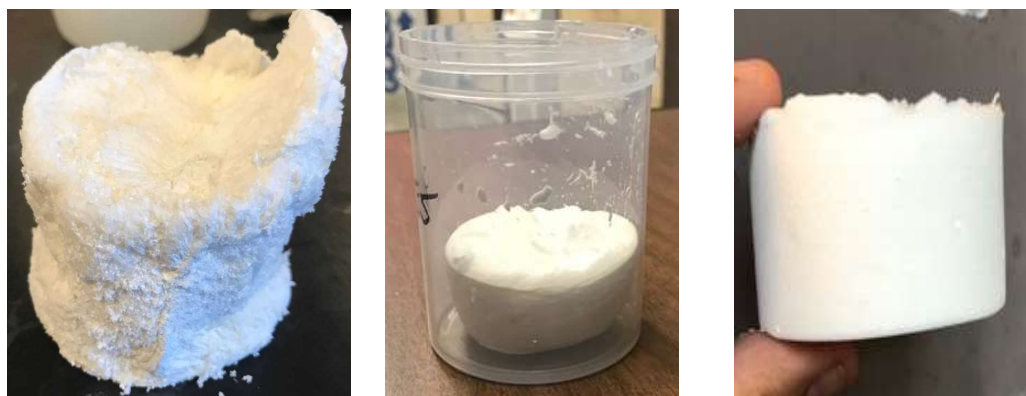


Figure 3.9 Collapse and shrinkage of FD-CNF cakes prepared from different solvent mixtures: *Left*, untreated CNF; *middle*, 5 wt% TBA; *right*, 20% TBA

FD w/ *n*-butanol (56 wt%) FD w/ *tert*-butanol (43 wt%) FD w/H₂O only



Figure 3.10 Colloidal stability of CNFs redispersed in water after freeze drying. Samples were allowed to stand for 24 hours after initial dispersion by sonication. *Left*, after FD with 56 wt% NBA; *middle*, after FD with 43 wt% TBA; *right*, no co-solvent added

The addition of *tert*-butyl alcohol (TBA) as a lyophilization co-solvent to CNF slurries greatly improved the quality of FD-CNFs, as compared with untreated slurries. The freeze-dried cakes produced from CNF slurries treated with 10 to 25 wt% TBA showed minimal collapse and shrinkage, suggestive of reduced hornification after lyophilization (Figure 3.11). Furthermore, the

colloidal stability of the FD-CNFs redispersed in water was vastly improved relative to dispersions of CNFs that were freeze-dried from untreated slurries (Figure 3.10). Interestingly, the improved cake structure is obtained only within a certain range of TBA concentrations, and begins to worsen above 25 wt% TBA. In addition to cake shrinkage at higher TBA concentrations, “lifting” of the sample from the bottom of the container could also be observed.



Figure 3.11 CNF cakes after freeze-drying from aqueous slurries containing 10 to 35 wt% TBA.

The co-solvent effect of added *n*-butanol (NBA) was studied as well, however addition of any amount of NBA produced serious deformations in cake appearance (Figure 3.12). It was concluded that NBA did not work nearly as well as TBA as a co-solvent during lyophilization.



Figure 3.12 Appearance of FD-CNF cakes from aqueous slurries containing 10–30 wt% NBA

SEM images of FD-CNFs produced from 10 and 20 wt% TBA showed increased porosity and a higher density of submicron fibers, relative to a freeze-dried sample prepared from an untreated slurry (Figure 3.13). BET measurements confirmed an increase in total surface area (Table 3.2).

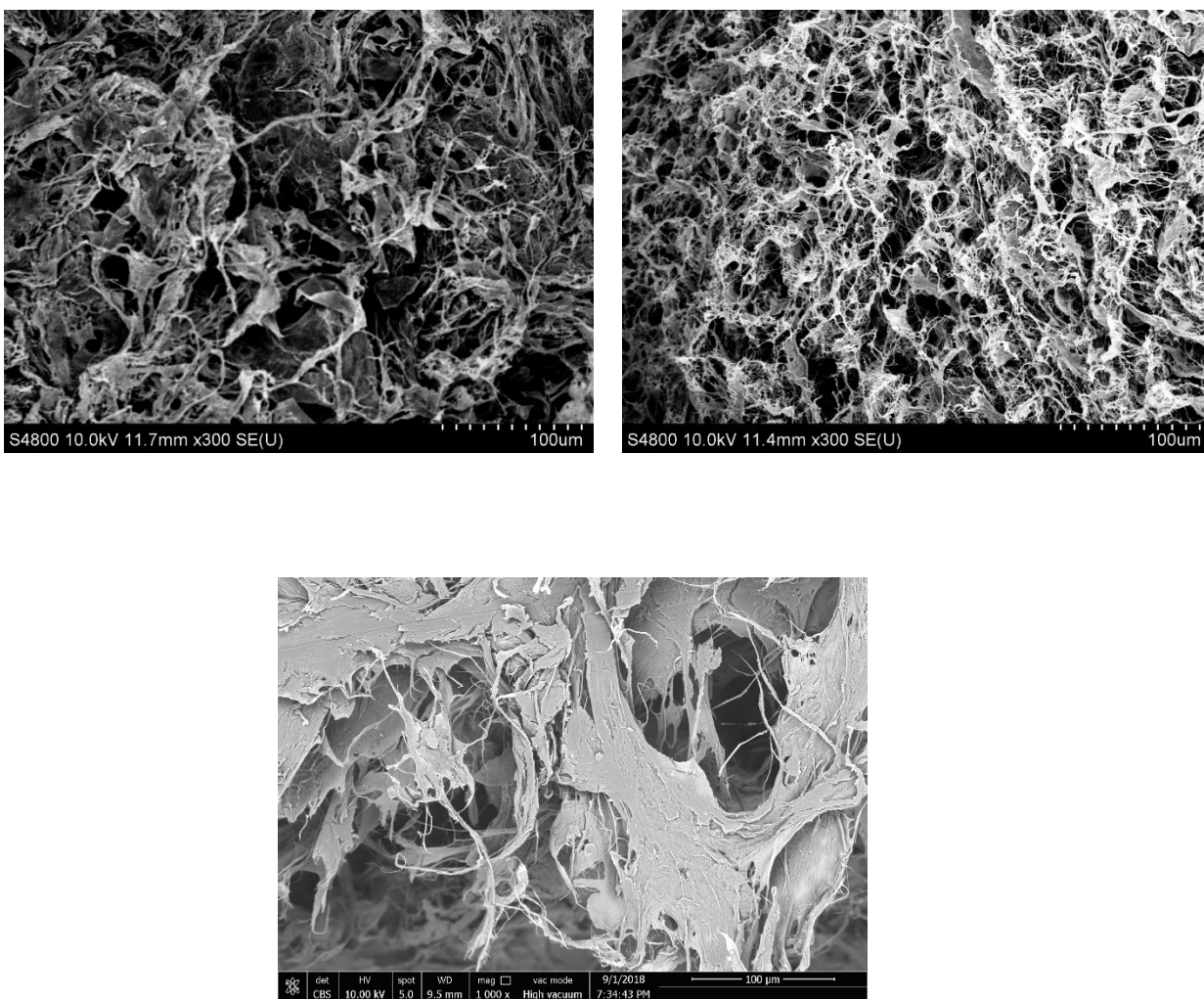


Figure 3.13 SEM images of freeze-dried CNFs. *Upper left*, FD-CNF lyophilized from 10 wt% TBA slurry; *upper right*, FD-CNF lyophilized from 20 wt% TBA slurry. Bottom, FD-CNF without TBA treatment. Images taken by Taehoo Chang.

Table 3.2 BET measurements of freeze-dried CNFs, as a function of initial TBA wt% prior to lyophilization. Data acquired by Taehoo Chang.

TBA %	Surface Area (m ² /g)
0	2.4432 ± 0.0288
10	23.4660 ± 0.1741
20	23.8307 ± 0.1731
30	20.4734 ± 0.1490
40	22.0818 ± 0.1367
50	19.5715 ± 0.1155

Lastly, freeze-dried CNFs were functionalized with lauric acid using mechanochemistry and dispersed as a 1 wt% chloroform solution. As expected, the use of CNFs lyophilized from slurries with 10% TBA resulted in much better dispersions in organic solvents after esterification, compared with CNFs obtained from untreated slurries (Figure 3.14).



Figure 3.14 Images (5 cm x 5 cm) of cast films prepared from 1 wt% laurylated CNF in chloroform. *Left*, prepared using CNFs lyophilized from water (untreated); *right*, prepared using CNFs lyophilized from slurries with 20 wt% TBA.

The relative DS values of grafted FD-CNFs lyophilized from 10% TBA (Table 3.3) were increased relative to those prepared from FD-CNFs without TBA (see Table 2.3), in accord with the increase in surface area due to TBA co-solvent effect. The prevention of fibrillar collapse would not only allow individual fibers to be separated, but also expose a greater number of surface hydroxyls for esterification. The resulting functionalized CNFs would benefit from higher density of chain grafting (accompanied by a decrease in surface hydroxyls) resulting in better dispersion in organic media such as CHCl_3 .

Table 3.3 DS value of esterified CNFs (lyophilized with 10% TBA as cosolvent)

Ester Type	DS
Caprylate (C6)	0.95
Laurate	1.08
Oleate (C18)	2.5
Benzoate	1.04
Pyroglutamate	0.16
Urocanate	0.14
Methacrylate	0.84
2-Furoate	0.81

3.5 Conclusion

The solventless modification of CNFs by mechanochemistry relies on the dewatering and controlled drying of CNFs from aqueous slurries. However, many attempts to speed up the drying process often result in hardened CNFs that could not be dispersed into finer powders. Solvent exchange with acetone and accelerated drying using heat or vacuum were both unsuccessful, although there may be some potential for their application toward novel structural materials.

The addition of TBA as a co-solvent to CNF slurries prior to freeze-drying greatly improved the dispersion properties of the resulting solid by limiting hornification and increasing surface area. SEM images revealed fewer and smaller aggregated bundles and a finer distribution of fiber widths, relative to CNFs freeze-dried from water. A systematic study of CNF microstructure as a function of solvent composition prior to lyophilization provided new insights into this field of inquiry. Indeed, the traditional description of a “good” cake is directly linked to CNF dispersion stability: cakes that showed collapse or shrinkage were less capable of producing stable colloidal solutions upon redispersion. CNF slurries containing 10–25 %TBA produced the best cakes after lyophilization, whose fibers were the least hornified and thus most readily redispersed. Lastly, MC esterification of powderized FD-CNFs prepared from 20% TBA slurries could be dispersed easily in CHCl_3 and cast into uniform films. In contrast, functionalization of FD-CNFs prepared from aqueous slurries produced grainy films with a high density of structural defects, due to extensive coagulation and agglomeration.

CHAPTER 4. STUDIES ON THE SUPERHYDROPHOBIC PROPERTIES OF FATTY ACID-ESTERIFIED CELLULOSE NANOFIBERS

4.1 Introduction to superhydrophobic materials

The use of TBA as a co-solvent in the preparation of FD-CNFs has led to improved fibrillation and dispersion stability of both unmodified and esterified CNFs dispersed in various solvents. Furthermore, the solvent-free, mechanochemical grafting of carboxylic acids onto FD-CNF surfaces enables the creation of uniform films that can be cast with various thicknesses. This presents a wonderful opportunity to study the wettability of coatings prepared from fatty acid-functionalized CNFs.

Wettability, a well-studied surface phenomenon,¹⁰⁶ describes the surface interaction between a liquid (usually water) and a solid surface. The degree of wettability can be quantified by the contact angle (CA) formed by a liquid droplet on solid surface (air–solid interface). An angle $< 90^\circ$ means that the liquid has some affinity for the surface (solvophilic), whereas an angle $> 90^\circ$ means the liquid is repelled by the surface (solvophobic).¹⁰⁷ In nature, surfaces of the lotus leaf and duck feathers are considered to be superhydrophobic (SHP) where the CA exceeds 150° and water droplets easily roll off the surface (Figure 4.1).¹⁰⁸ Furthermore, if the surface on which the liquid rests is tilted, the *sliding angle* becomes a useful parameter to define wettability. The sliding angles of SHP surfaces are considered to be smaller than 5° .¹¹⁰

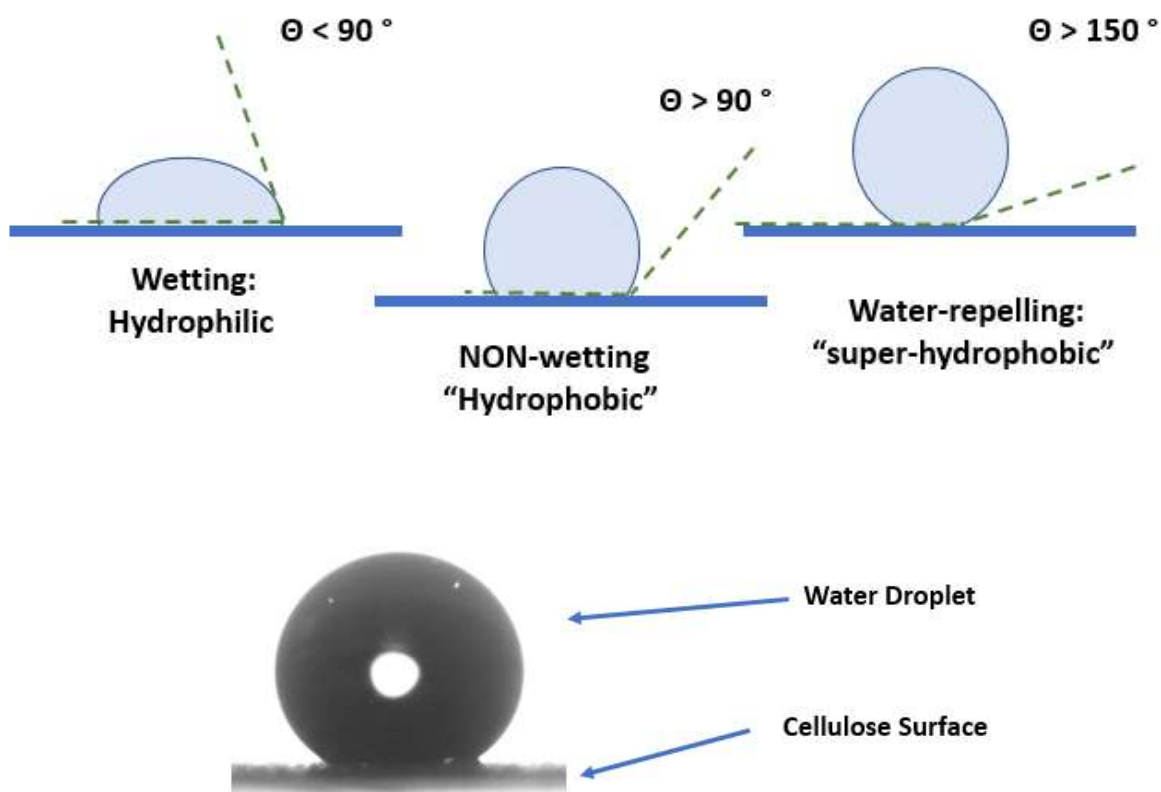


Figure 4.1 (Above) Contact angles for hydrophilic, hydrophobic and superhydrophobic (SHP) surfaces supporting a water droplet. (Below) Photo of a water droplet on a SHP-CNF surface.

Immediate applications of SHP surfaces include self-cleaning materials,¹¹¹ anti-fogging windows,¹¹² and ship bottoms with reduced drag¹¹³ to name a few. An extensive review by Mageshwaran for recent applications of SHP surfaces is recommended.¹¹⁴

The qualities responsible for SHP surfaces can be chemical, physical or a combination of both. Chemical modification alters the interactions between liquid and surface; simply put, the surface energy is lowered. However, chemical modification (such as surface grafting with fatty acids, as described in the previous chapter) is not enough on its own to overcome the CA threshold of 150° that defines SHP, although it can bring the CA to 130° .¹¹⁵

Physical structure is also important for SHP. In order to better understand these, two working models have been established. The Wenzel model¹¹⁶ assumes a conformal contact between liquid and solid surfaces (i.e., no air pockets are created), whereas the Cassie or Cassie–Baxter model¹¹⁷ invokes surface tension between liquid and gas, such that the liquid touches only the edges and vertices of solid surfaces with pockets of gas trapped underneath (Figure 4.2). The latter model emphasizes the importance of surface roughness: An imaginative take on surface roughness is the planet Earth with its mountain ranges and forests. From afar the surface looks smooth, but closer inspection shows valleys and peaks. Thus, most SHP surfaces exhibit microscopic features with minimum contact with the water drop, which is supported from below by the pressure created by the air/gas pockets.

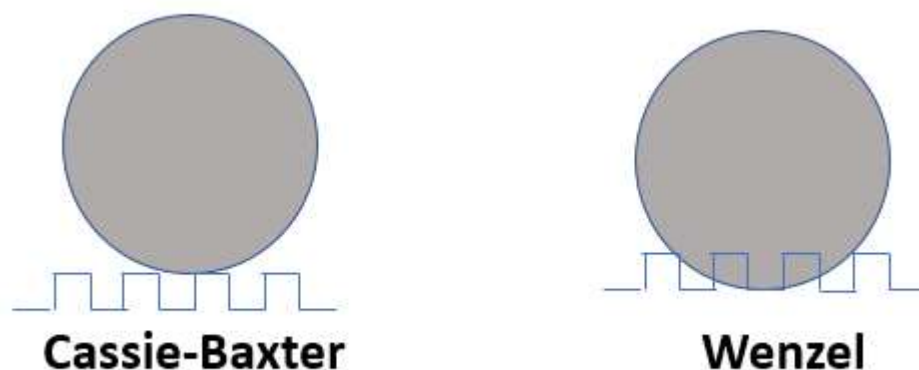


Figure 4.2 The two physical models used to explain wetting phenomena at the air/liquid/solid interface.

4.2 Generating Cellulose Nanomaterials with Hydrophobic Surfaces

Nanocellulose fibers provide an opportunity to produce biorenewable SHP materials, which have caught the attention of the scientific community.¹¹⁸⁻¹²² The advantages of nanoscale materials includes more surface area for chemical modification and finer structural features that support the Cassie–Baxter model. To date, efforts to prepare SHP surfaces either involve the deposition of materials as coatings or thin films, or the generation of microtextured surfaces by lithographic methods.¹²⁰ However, most SHP surfaces are limited by abrasion or fouling, and need to be replaced or reapplied.

One method of reducing the surface energy of cellulose-based substrates is to sprinkle nanoparticles (NP) onto cellulose fibers to produce composite materials with SiO₂, ZnO, or Ag NPs (which has also found use as a catalyst support).¹²³ Innovative and functional as these are, underlying issues of environmental toxicity and cost (reagents and equipment) still need to be addressed.

The culmination of experimental work in this thesis supports a simple and reproducible process for creating eco-friendly SHP coatings from chemically modified CNFs, using methods that are scalable and cost-effective. The SHP coatings can also be regenerated after damage or fouling by exfoliation, which is important for practical applications: while SHP surfaces produced by living systems naturally repair themselves, synthetic SHP surfaces are generally not self-renewable. SHP surfaces were characterized by FTIR, solid-state ¹³C NMR, contact-angle measurements, and SEM analysis, the latter two in collaboration with Taehoo Chang.

4.3 Experimental

Preparation of materials

In a typical procedure, 1 gram of esterified CNFs just after MC synthesis (see Chapter 3) was placed in a 200-mL Erlenmeyer flask, suspended in 100 mL EtOH, and stirred for 30 minutes at room temperature. The product was collected via Buchner funnel lined with a 90-mm paper disk (Whatman 1), washed with EtOH (3 x 10 mL), then flushed with air. The disk of esterified CNFs was carefully removed from the paper, and allowed to dry in air on a watch glass.

Wetting analysis and exfoliation

Freshly prepared CNF disks (see procedure above) or squares mounted on glass slides were tested for hydrophobicity and SHP by depositing a water droplet onto the CNF surface with a syringe, with the substrate positioned at various slant angles. Exfoliation of CNF substrates was performed by laying cellophane tape (Scotch) over the surface, followed by its removal using a peeling motion to expose a fresh layer.

4.4 Results and Discussion

In reference to the work presented in Chapter 3, fatty-acid grafted CNFs prepared by the freeze drying of aqueous slurries with 10 wt% TBA provide an interesting segue into SHP materials. This simple method of functionalizing CNF surfaces involves low-cost reagents and minimum solvent, and sets the stage for processes that can be performed on an industrial scale.

Initial studies were performed with oleic acid-functionalized CNFs. It was hypothesized that in addition to its inherently hydrophobic character, the internal double bond in the fatty acid chain introduces a “kink” that prevents its dense packing. In contrast, the fully saturated stearic

acid readily adopts a linear conformation and can pack closely with neighboring molecules, as is evident from its higher melting point versus oleic acid (Figure 4.3).

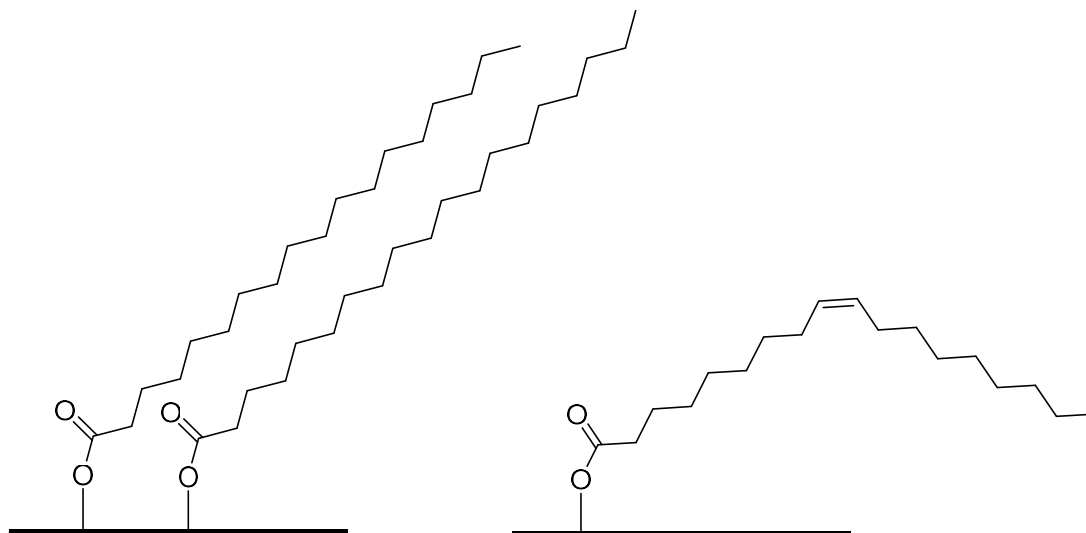


Figure 4.3 *Above*, stearoyl versus oleyl chains grafted on CNF surfaces; *below*, disk of oleyl-CNF after filtering and drying

Wetting experiments were conducted first on disks of oleylated CNFs, prepared by filtering, washing, and drying in a Buchner funnel (Figure 4.4). This material meets the basic criteria for superhydrophobicity: free-standing water droplets moved around freely, and quickly slid off the disk at a slight tilt angle. Few if any water droplets were pinned at any part of the membrane, indicated that the entire surface exhibited SHP character.



Figure 4.4 Freely moving water droplets on oleylated CNF disk

The disks prepared by collection of oleyl-CNFs on filter paper were at least 100 micrometers thick. To test the ability to cast CNFs into SHP thin films on thermoplastic substrates such as PET, oleylated CNFs were suspended in CHCl_3 or EtOH for deposition by spray coating. The latter proved harder to disperse and caused clogging at the spray gun, however, thin films could be produced by spraying CHCl_3 dispersions of oleyl-CNF onto PET films, which exhibited SHP in subsequent wetting tests (Figure 4.5).

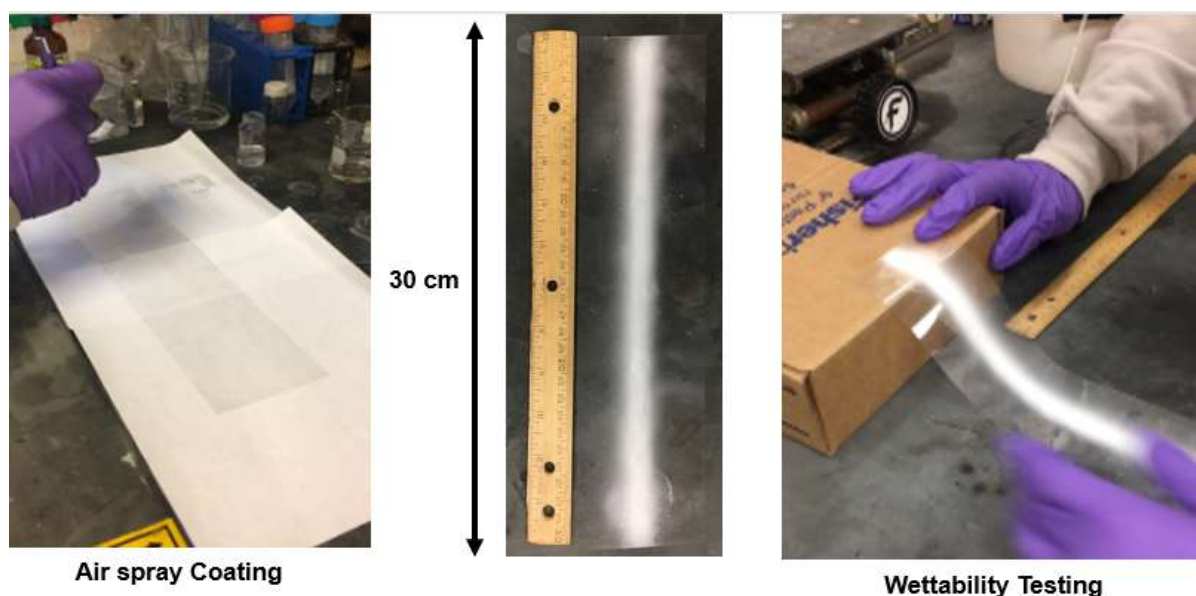


Figure 4.5. Spray coating of oleyl-CNF onto PET film; a SHP coating was formed after several passes. SHP demonstrations were performed by placing the coated PET at an incline.

Static contact angles were measured on four different spray-coated samples, prepared from surface-modified CNFs using fatty acids having different chain lengths: (1) hexanoic acid (C6-CNF), (2) lauric acid (C12-CNF), (3) stearic acid (C18-CNF), and (4) oleic acid (OA-CNF; Figure 4.6 and Table 4.1). Three out of four CNF samples exhibited SHP character, whereas C18-CNFs coatings were simply hydrophobic. The differences in sample wettability can be attributed in part to the dense chain packing in C18-CNFs represented in Figure 4.3; the limited freedom of the alkyl chains reduces their ability to provide effective steric repulsion against fiber aggregation. On the other hand, OA-CNF (monounsaturated C18-CNF) had the highest static contact angle. SEM image of spraying coated OA-CNF indicated a fibrous hierarchical structure with micro/nano sized pores (Figure 4.7).

Table 4.1 Static contact angles for spray-coated CNG thin films on PET substrates. Data collected by Taehoo Chang.

Material	CA (static)
C ₆ -CNF	157.2 ± 2.0
C ₁₂ -CNF	157.6 ± 0.4
C ₁₈ -CNF	130.7 ± 4.8
OA-CNF	159.9 ± 2.3

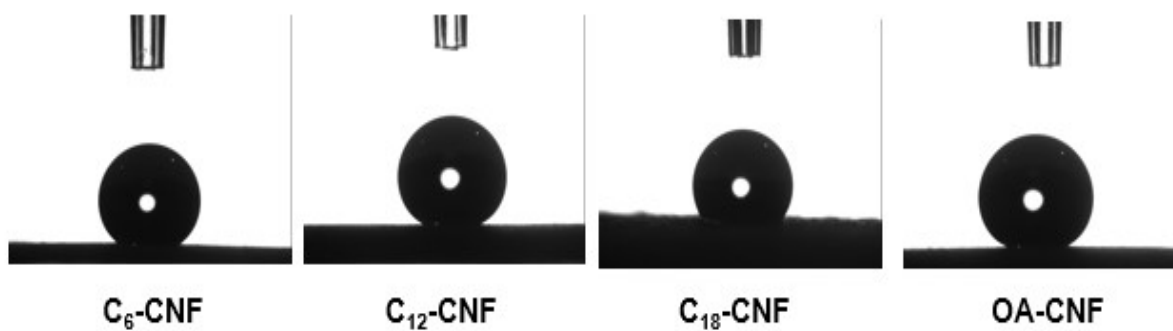


Figure 4.6 Water droplet dispensed onto functionalized CNF surfaces. Photos taken by Taehoo Chang.

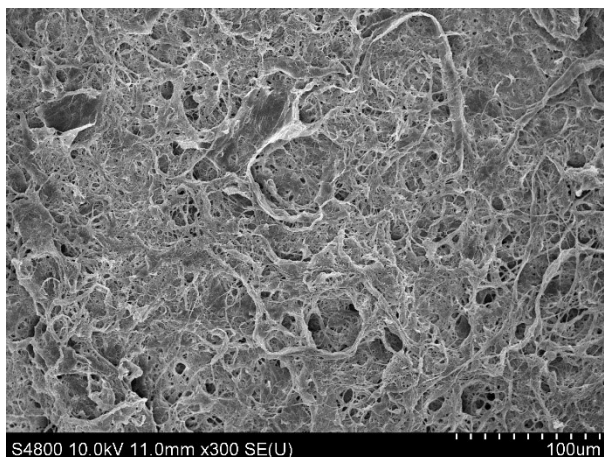


Figure 4.7 SEM image of oleyl-CNFs spray-coated onto PET substrate. Image taken by Taehoo Chang.

The SHP properties of the CNF-coated samples can be compromised by physical defects or fouling. For example, a pad of OA-CNF mounted on a glass slide exhibited SHP character, as expected (Figure 4.8). However, scratching or touching the surface with an unwashed thumb resulted in a loss of SHP. This property could be recovered by exfoliating the CNF sample with Scotch tape, revealing a fresh and unblemished OA-CNF surface, which demonstrates an ability to regenerate SHP that could be useful in applications such as self-cleaning surfaces.



A



B



C



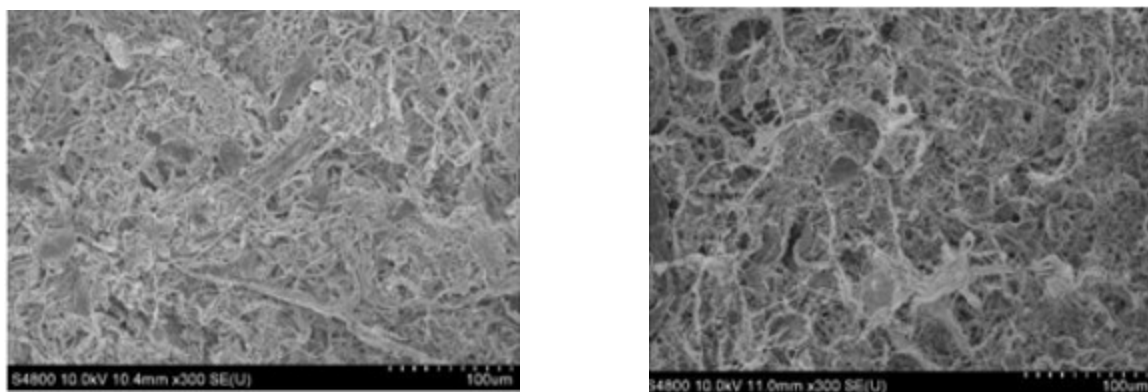
D



E

Figure 4.8 (A) Olelylated CNF mounted on a glass slide showing SHP behavior; (B) pressing sample with unwashed thumb; (C) loss of SHP due to contaminated surface; (D) exfoliation of surface with Scotch tape; (E) restoration of SHP using exfoliated sample on glass slide, and also reverse side of tape.

The SHP properties of OA-CNF coatings do not appear to be degraded by simple compression. The roughness of the OA-CNF surface is reduced after a compressive force is applied (Figure 4.9A), however SHP is still retained. Exfoliation restores the original surface roughness without loss of SHP character (Figure 4.9B).



A

B

Figure 4.9 (A) SEM image of OA-CNF after compression with gloved thumb; (B) recovery of surface roughness after exfoliation. Images taken by Taehoo Chang.

4.5 Conclusion

The methodology developed for the mechanochemistry and processing of fatty-acid modified nanocellulose fibers afforded homogenous SHP films that produced contact angles that superseded 150° . Physical damage or chemical fouling of the CNF surfaces causes a loss in their SHP character, but this can be recovered by a simple exfoliation step. The hierarchical structure of the CNF films is likely an important feature in the regeneration of SHP function. Future work in characterizing and modeling SHP CNF surfaces are currently underway.

REFERENCES

1. Council, N. R., in *Sustainability and the U.S. EPA*. The National Academies Press: Washington, DC, 2011; p 162.
2. Anastas, P. T.; Williamson, T. C., Green chemistry: An overview. *ACS Symposium Series* **1996**, *626*, 1-17.
3. Cellulose. In *Kirk-Othmer Encyclopedia of Chemical Technology*.
4. Dai, D.; Fan, M.; Collins, P., Fabrication of nanocelluloses from hemp fibers and their application for the reinforcement of hemp fibers. *Industrial Crops and Products* **2013**, *44*, 192-199.
5. Mandal, A.; Chakrabarty, D., Isolation of nanocellulose from waste sugarcane bagasse (SCB) and its characterization. *Carbohydrate Polymers* **2011**, *86* (3), 1291-1299.
6. Barbash, V.; Yashchenko, O.; Kedrovska, A., *Preparation and Properties of Nanocellulose from Peracetic Flax Pulp*. 2017; Vol. 16, p 1-10.
7. Theivasanthi, T.; Anne Christma, F. L.; Toyin, A. J.; Gopinath, S. C. B.; Ravichandran, R., Synthesis and characterization of cotton fiber-based nanocellulose. *International Journal of Biological Macromolecules* **2018**, *109*, 832-836.
8. Klemm, D.; Schumann, D.; Udhardt, U.; Marsch, S., Bacterial synthesized cellulose — artificial blood vessels for microsurgery. *Progress in Polymer Science* **2001**, *26* (9), 1561-1603.
9. Sano, M. B.; Rojas, A. D.; Gatenholm, P.; Davalos, R. V., Electromagnetically controlled biological assembly of aligned bacterial cellulose nanofibers. *Annals of Biomedical Engineering* **2010**, *38* (8), 2475-84.
10. Feng, X.; Ullah, N.; Wang, X.; Sun, X.; Li, C.; Bai, Y.; Chen, L.; Li, Z., Characterization of Bacterial Cellulose by *Gluconacetobacter hansenii* CGMCC 3917. *Journal of Food Science* **2015**, *80* (10), E2217-27.
11. Moniri, M.; Boroumand Moghaddam, A.; Azizi, S.; Abdul Rahim, R.; Bin Ariff, A.; Zuhainis Saad, W.; Navaderi, M.; Mohamad, R., Production and Status of Bacterial Cellulose in Biomedical Engineering. *Nanomaterials* **2017**, *7* (9), 257.
12. Zhao, Y.; Li, J. J. C., Excellent chemical and material cellulose from tunicates: diversity in cellulose production yield and chemical and morphological structures from different tunicate species. *Cellulose* **2014**, *21* (5), 3427-3441.

13. Lavanya, D.; Kulkarni, P.; Dixit, M.; Raavi, P. K.; Krishna, L. N. V., in Sources of cellulose and their applications- A review. *International Journal of Drug Formulation and Research* **2011**; Vol. 2, p 19-38.
14. Klemm, D.; Heublein, B.; Fink, H.-P.; Bohn, A., Cellulose: Fascinating Biopolymer and Sustainable Raw Material. *Angewandte Chemie International Edition* **2005**, *44* (22), 3358-3393.
15. Habibi, Y., Key advances in the chemical modification of nanocelluloses. *Chemical Society Reviews* **2014**, *43* (5), 1519-1542.
16. Pfister, D. H., American canopy: trees, forests, and the making of a nation. *Choice: Current Reviews for Academic Libraries* **2012**, *50* (4)
17. Berglund, L. A.; Burgert, I., Bioinspired Wood Nanotechnology for Functional Materials. *Advanced Materials* **2018**, *30* (19), 1-15.
18. Jose Chirayil, C.; Mathew, L.; Thomas, S., in Review of recent research in nano cellulose preparation from different lignocellulosic fibers. *Reviews on advanced materials science* **2014**; Vol. 37, p 20-28.
19. Thomas, B.; Raj, M. C.; B, A. K.; H, R. M.; Joy, J.; Moores, A.; Drisko, G. L.; Sanchez, C., Nanocellulose, a Versatile Green Platform: From Biosources to Materials and Their Applications. *Chemical Reviews* **2018**, *118* (24), 11575-11625.
20. George, J.; Sabapathi, S. N., Cellulose nanocrystals: synthesis, functional properties, and applications. *Nanotechnology, Science and Applications* **2015**, *8*, 45-54.
21. The Biosynthesis of Cellulose AU - Brown, R. Malcolm. *Journal of Macromolecular Science, Part A* **1996**, *33* (10), 1345-1373.
22. Nogi, M.; Iwamoto, S.; Nakagaito, A. N.; Yano, H., Optically Transparent Nanofiber Paper. *Advanced Materials* **2009**, *21* (16), 1595-1598.
23. Islam, M.; Mahbubul Alam, M.; Zoccola, M., International Journal of Innovate Research in Science Engineering and Technoloy. *Review on modification of nanocellulose for application in composites*. **2013**; Vol. 2, p 5445.
24. Melik, D. H.; Fogler, H. S., Colloidal Stability: Comparison of Sedimentation with Sedimentation Flocculation. In *Macro- and Microemulsions*, ACS Publications **1985**; Vol. 272, pp 461-470.
25. Eyley, S.; Thielemans, W., Surface modification of cellulose nanocrystals. *Nanoscale* **2014**, *6* (14), 7764-7779.
26. Peng, S. X.; Chang, H.; Kumar, S.; Moon, R. J.; Youngblood, J. P., A comparative guide to controlled hydrophobization of cellulose nanocrystals via surface esterification. *Cellulose* **2016**, *23* (3), 1825-1846.

27. Isogai, A.; Saito, T.; Fukuzumi, H., TEMPO-oxidized cellulose nanofibers. *Nanoscale* **2011**, *3* (1), 71-85.
28. Kim, U.-J.; Kuga, S.; Wada, M.; Okano, T.; Kondo, T., Periodate Oxidation of Crystalline Cellulose. *Biomacromolecules* **2000**, *1* (3), 488-492.
29. Yoo, Y.; Youngblood, J. P., Green One-Pot Synthesis of Surface Hydrophobized Cellulose Nanocrystals in Aqueous Medium. *ACS Sustainable Chemistry & Engineering* **2016**, *4* (7), 3927-3938.
30. Lu, P.; Hsieh, Y.-L., Preparation and properties of cellulose nanocrystals: Rods, spheres, and network. *Carbohydrate Polymers* **2010**, *82* (2), 329-336.
31. Filson, P. B.; Dawson-Andoh, B. E.; Schwegler-Berry, D., Enzymatic-mediated production of cellulose nanocrystals from recycled pulp. *Green Chemistry* **2009**, *11* (11), 1808-1814.
32. Revol, J. F.; Bradford, H.; Giasson, J.; Marchessault, R. H.; Gray, D. G., Helicoidal self-ordering of cellulose microfibrils in aqueous suspension. *International Journal of Biological Macromolecules* **1992**, *14* (3), 170-172.
33. Xu, X.; Liu, F.; Jiang, L.; Zhu, J. Y.; Haagenson, D.; Wiesenborn, D. P., Cellulose Nanocrystals vs. Cellulose Nanofibrils: A Comparative Study on Their Microstructures and Effects as Polymer Reinforcing Agents. *ACS Applied Materials & Interfaces* **2013**, *5* (8), 2999-3009.
34. Morgenstein, M. E.; Redmount, C. A., Mudbrick Typology, Sources, and Sedimentological Composition: A Case Study from Tell el-Muqdam, Egyptian Delta. *Journal of the American Research Center in Egypt* **1998**, *35*, 129-146.
35. Yano, H.; Omura, H.; Honma, Y.; Okumura, H.; Sano, H.; Nakatsubo, F., Designing cellulose nanofiber surface for high density polyethylene reinforcement. *Cellulose* **2018**, *25* (6), 3351-3362.
36. Wang, T.; Drzal, L. T., Cellulose-Nanofiber-Reinforced Poly(lactic acid) Composites Prepared by a Water-Based Approach. *ACS Applied Materials & Interfaces* **2012**, *4* (10), 5079-5085.
37. Chen, C.; Mo, M.; Chen, W.; Pan, M.; Xu, Z.; Wang, H.; Li, D., Highly conductive nanocomposites based on cellulose nanofiber networks via NaOH treatments. *Composites Science and Technology* **2018**, *156*, 103-108.
38. Serizawa, T.; Sawada, T.; Okura, H.; Wada, M., Hydrolytic Activities of Crystalline Cellulose Nanofibers. *Biomacromolecules* **2013**, *14* (3), 613-617.
39. Shin, S.; Hyun, J., Matrix-Assisted Three-Dimensional Printing of Cellulose Nanofibers for Paper Microfluidics. *ACS Applied Material and Interfaces* **2017**, *9* (31), 26438-26446.

40. Takacs, L., The historical development of mechanochemistry. *Chemical Society Reviews* **2013**, *42* (18), 7649-7659.
41. Beyer, M. K.; Clausen-Schaumann, H., Mechanochemistry: The Mechanical Activation of Covalent Bonds. *Chemical Reviews* **2005**, *105* (8), 2921-2948.
42. Hasa, D.; Jones, W., Screening for new pharmaceutical solid forms using mechanochemistry: A practical guide. *Advanced Drug Delivery Reviews* **2017**, *117*, 147-161.
43. Suryanarayana, C., Mechanical alloying and milling. *Progress in Materials Science* **2001**, *46* (1), 1-184.
44. Bolm, C.; Hernández, J. G., Mechanochemistry of Gaseous Reactants. *Angewandte Chemie International Edition* **2019**, *58*, 3285-3299
45. Wang, G.-W., Mechanochemical organic synthesis. *Chemical Society Reviews* **2013**, *42* (18), 7668-7700.
46. Kubota, K.; Seo, T.; Koide, K.; Hasegawa, Y.; Ito, H., Olefin-accelerated solid-state C–N cross-coupling reactions using mechanochemistry. *Nature Communications* **2019**, *10* (1), 111.
47. Takacs, L., The Father of Mechanochemistry. *Bulletin for the History of Chemistry* **2004**, *28*, 26-34.
48. Hernández, J. G.; Bolm, C., Altering Product Selectivity by Mechanochemistry. *The Journal of Organic Chemistry* **2017**, *82* (8), 4007-4019.
49. Katsenis, A. D.; Puškarić, A.; Štrukil, V.; Mottillo, C.; Julien, P. A.; Užarević, K.; Pham, M.-H.; Do, T.-O.; Kimber, S. A. J.; Lazić, P.; Magdysyuk, O.; Dinnebier, R. E.; Halasz, I.; Friščić, T., In situ X-ray diffraction monitoring of a mechanochemical reaction reveals a unique topology metal-organic framework. *Nature Communications* **2015**, *6*, 6662.
50. Friščić, T.; Halasz, I.; Beldon, P. J.; Belenguer, A. M.; Adams, F.; Kimber, S. A. J.; Honkimäki, V.; Dinnebier, R. E., Real-time and in situ monitoring of mechanochemical milling reactions. *Nature Chemistry* **2012**, *5*, 66.
51. Thiessen, P. A. M., K.; Heinicke, G., Grundlagen Der Tribochemie *Akademie-Verlag* **1967**, *1*
52. Do, J.-L.; Friščić, T., Mechanochemistry: A Force of Synthesis. *ACS Central Science* **2017**, *3* (1), 13-19.
53. Muñoz-Batista, M. J.; Rodriguez-Padron, D.; Puente-Santiago, A. R.; Luque, R., Mechanochemistry: Toward Sustainable Design of Advanced Nanomaterials for Electrochemical Energy Storage and Catalytic Applications. *ACS Sustainable Chemistry & Engineering* **2018**, *6* (8), 9530-9544.

54. Stauch, T.; Dreuw, A., Advances in Quantum Mechanochemistry: Electronic Structure Methods and Force Analysis. *Chemical Reviews* **2016**, *116* (22), 14137-14180.
55. Fleming, I., *Molecular Orbitals and Organic Chemical Reactions*. Wiley: 2010.
56. McKissic, K. S.; Caruso, J. T.; Blair, R. G.; Mack, J., Comparison of shaking versus baking: further understanding the energetics of a mechanochemical reaction. *Green Chemistry* **2014**, *16* (3), 1628-1632.
57. Stolle, A.; Szuppa, T.; Leonhardt, S. E. S.; Ondruschka, B., Ball milling in organic synthesis: solutions and challenges. *Chemical Society Reviews* **2011**, *40* (5), 2317-2329.
58. Kulla, H.; Wilke, M.; Fischer, F.; Röllig, M.; Maierhofer, C.; Emmerling, F., Warming up for mechanosynthesis – temperature development in ball mills during synthesis. *Chemical Communications* **2017**, *53* (10), 1664-1667.
59. Užarević, K.; Štrukil, V.; Mottillo, C.; Julien, P. A.; Puškarić, A.; Friščić, T.; Halasz, I., Exploring the Effect of Temperature on a Mechanochemical Reaction by in Situ Synchrotron Powder X-ray Diffraction. *Crystal Growth & Design* **2016**, *16* (4), 2342-2347.
60. Andersen, J. M.; Mack, J., Decoupling the Arrhenius equation via mechanochemistry. *Chemical Science* **2017**, *8* (8), 5447-5453.
61. Zhang, F.; Qiu, W.; Yang, L.; Endo, T.; Hirotsu, T., Mechanochemical preparation and properties of a cellulose–polyethylene composite. *Journal of Materials Chemistry* **2002**, *12* (1), 24-26.
62. Huang, P.; Wu, M.; Kuga, S.; Wang, D.; Wu, D.; Huang, Y., One-Step Dispersion of Cellulose Nanofibers by Mechanochemical Esterification in an Organic Solvent. *ChemSusChem* **2012**, *5* (12), 2319-2322.
63. Kang, X.; Sun, P.; Kuga, S.; Wang, C.; Zhao, Y.; Wu, M.; Huang, Y., Thin Cellulose Nanofiber from Corncob Cellulose and Its Performance in Transparent Nanopaper. *ACS Sustainable Chemistry & Engineering* **2017**, *5* (3), 2529-2534.
64. Foster, E. J.; Moon, R. J.; Agarwal, U. P.; Bortner, M. J.; Bras, J.; Camarero-Espinosa, S.; Chan, K. J.; Clift, M. J. D.; Cranston, E. D.; Eichhorn, S. J.; Fox, D. M.; Hamad, W. Y.; Heux, L.; Jean, B.; Korey, M.; Nieh, W.; Ong, K. J.; Reid, M. S.; Renneckar, S.; Roberts, R.; Shatkin, J. A.; Simonsen, J.; Stinson-Bagby, K.; Wanasekara, N.; Youngblood, J., Current characterization methods for cellulose nanomaterials. *Chemical Society Reviews* **2018**, *47* (8), 2609-2679.
65. Elazzouzi-Hafraoui, S.; Nishiyama, Y.; Putaux, J.-L.; Heux, L.; Dubreuil, F.; Rochas, C., The Shape and Size Distribution of Crystalline Nanoparticles Prepared by Acid Hydrolysis of Native Cellulose. *Biomacromolecules* **2008**, *9* (1), 57-65.
66. Berlioz, S.; Molina-Boisseau, S.; Nishiyama, Y.; Heux, L., Gas-Phase Surface Esterification of Cellulose Microfibrils and Whiskers. *Biomacromolecules* **2009**, *10* (8), 2144-2151.

67. Xiao, L.; Mai, Y.; He, F.; Yu, L.; Zhang, L.; Tang, H.; Yang, G., Bio-based green composites with high performance from poly(lactic acid) and surface-modified microcrystalline cellulose. *Journal of Materials Chemistry* **2012**, *22* (31), 15732-15739.
68. Lanzillotto, M.; Konnert, L.; Lamaty, F.; Martinez, J.; Colacino, E., Mechanochemical 1,1-Carbonyldiimidazole-Mediated Synthesis of Carbamates. *ACS Sustainable Chemistry & Engineering* **2015**, *3* (11), 2882-2889.
69. Paul, R.; Anderson, G. W., N,N'-Carbonyldiimidazole, a New Peptide Forming Reagent. *Journal of the American Chemical Society* **1960**, *82* (17), 4596-4600.
70. Montalbetti, C. A. G. N.; Falque, V., Amide bond formation and peptide coupling. *Tetrahedron* **2005**, *61* (46), 10827-10852.
- 71a. Bennett, A. E.; Rienstra, C. M.; Auger, M.; Lakshmi, K. V.; Griffin, R. G., Heteronuclear Decoupling in Rotating Solids. *Journal of Chemical Physics* **1995**, *103* (16), 6951-6958.
- 71b. Dixon, W. T.; Schaefer, Jacob.; Sefcik, M. D.; Stejskal, E.; O.McKay, R. A.; Total suppression of sidebands in CPMAS C-13 NMR. *Journal of Magnetic Resonance* **1969**, *49* (2), 341-345.
72. Menon, M. P.; Selvakumar, R.; Kumar, P. S.; Ramakrishna, S., Extraction and modification of cellulose nanofibers derived from biomass for environmental application. *RSC Advances* **2017**, *7* (68), 42750-42773.
73. Zimmermann, M. V. G.; Borsoi, C.; Lavoratti, A.; Zanini, M.; Zattera, A. J.; Santana, R. M. C., Drying techniques applied to cellulose nanofibers. *Journal of Reinforced Plastics and Composites* **2016**, *35* (8), 628-643.
74. Peng, Y. C.; Gardner, D. J.; Han, Y. S., Drying cellulose nanofibrils: in search of a suitable method. *Cellulose* **2012**, *19* (1), 91-102.
75. Oksman, K.; Aitomaki, Y.; Mathew, A. P.; Siqueira, G.; Zhou, Q.; Butylina, S.; Tanpichai, S.; Zhou, X. J.; Hooshmand, S., Review of the recent developments in cellulose nanocomposite processing. *Composites Part A-Applied Science and Manufacturing* **2016**, *83*, 2-18.
76. Fernandes Diniz, J. M. B.; Gil, H.; Castro, J. A. A. M., Hornification—its origin and interpretation in wood pulps. *Wood Science and Technology* **2004**, *37*, 489-494.
77. Lovikka, V. A.; Khanjani, P.; Väisänen, S.; Vuorinen, T.; Maloney, T. C., Porosity of wood pulp fibers in the wet and highly open dry state. *Microporous and Mesoporous Materials* **2016**, *234*, 326-335.
78. Ciftci, D.; Ubeyitogullari, A.; Huerta, R. R.; Ciftci, O. N.; Flores, R. A.; Saldana, M. D. A., Lupin hull cellulose nanofiber aerogel preparation by supercritical CO₂ and freeze drying. *The Journal of Supercritical Fluids* **2017**, *127*, 137-145.

79. Kolakovic, R.; Peltonen, L.; Laaksonen, T.; Putkisto, K.; Laukkanen, A.; Hirvonen, J., Spray-Dried Cellulose Nanofibers as Novel Tablet Excipient. *American Association of Pharmaceutical Scientists* **2011**, *12* (4), 1366-1373.
80. Cervin, N. T.; Johanson, E.; Larsson, P. A.; Wagberg, L., Strong, Water-Durable, and Wet-Resilient Cellulose Nanofibril-Stabilized Foams from Oven Drying. *ACS Applied Materials & Interfaces* **2016**, *8* (18), 11682-11689.
81. Nemoto, J.; Saito, T.; Isogai, A., Simple Freeze-Drying Procedure for Producing Nanocellulose Aerogel-Containing, High-Performance Air Filters. *ACS Applied Materials & Interfaces* **2015**, *7* (35), 19809-19815.
82. Beckman, E. J., Supercritical and near-critical CO₂ in green chemical synthesis and processing. *The Journal Supercritical Fluids* **2004**, *28* (2-3), 121-191.
83. Vicente, J.; Pinto, J.; Menezes, J.; Gaspar, F., Fundamental analysis of particle formation in spray drying. *Powder Technology* **2013**, *247*, 1-7.
84. Gohel, M.; Parikh, R. K.; Nagori, S. A.; Gandhi, A. V.; Shroff, M. S.; Patel, P. K.; Gandhi, C. S.; Patel, V.; Bhagat, N. Y.; Poptani, S. D.; Kharadi, S. R.; Pandya, R.; Patel, T. C., Spray drying: A review *Pharmaceutical Reviews*. 2009; Vol. 7, 2-23.
85. Weise, U.; Maloney, T.; Paulapuro, H., Quantification of water in different states of interaction with wood pulp fibres. *Cellulose* **1996**, *3* (4), 189-202.
86. Belle, J.; Odermatt, J., Initial wet web strength of paper. *Cellulose* **2016**, *23* (4), 2249-2272.
87. Bhambere, D.; A. Gaidhani, K.; Harwalkar, M.; S. Nirgude, P., Lyophilization/Freeze Drying - A Review. *International Journal of Novel Trends in Pharamecutical Sciences* **2015**; Vol. 4, p 516-543.
88. Patel, S. M.; Doen, T.; Pikal, M. J., Determination of end point of primary drying in freeze-drying process control. *American Association of Pharmaceutical Scientists* **2010**, *11* (1), 73-84.
89. Wagner, W., International Equations for the Pressure Along the Melting and Along the Sublimation Curve of Ordinary Water Substance. *Journal of Physical and Chemical Reference Data* **1994**, *23* (3), 515-525.
90. Atkins, P.; de Paula, J., *Atkins' Physical Chemistry*. OUP Oxford: 2010.
91. Beirowski, J.; Inghelbrecht, S.; Arien, A.; Gieseler, H., Freeze drying of nanosuspensions, 2: the role of the critical formulation temperature on stability of drug nanosuspensions and its practical implication on process design. *Journal of Pharmaceutical Sciences* **2011**, *100* (10), 4471-4481.
92. Long, L. Y.; Weng, Y. X.; Wang, Y. Z., Cellulose Aerogels: Synthesis, Applications, and Prospects. *Polymers (Basel)* **2018**, *10* (6), 1-28.

93. De France, K. J.; Hoare, T.; Cranston, E. D., Review of Hydrogels and Aerogels Containing Nanocellulose. *Chemistry of Materials* **2017**, *29* (11), 4609-4631.
94. Han, J.; Zhou, C.; Wu, Y.; Liu, F.; Wu, Q., Self-Assembling Behavior of Cellulose Nanoparticles during Freeze-Drying: Effect of Suspension Concentration, Particle Size, Crystal Structure, and Surface Charge. *Biomacromolecules* **2013**, *14* (5), 1529-1540.
95. Hottot, A.; Vessot, S.; Andrieu, J., Freeze drying of pharmaceuticals in vials: Influence of freezing protocol and sample configuration on ice morphology and freeze-dried cake texture. *Chemical Engineering and Processing: Process Intensification* **2007**, *46* (7), 666-674.
96. *Freeze-drying/lyophilization of pharmaceutical and biological products*, 2nd ed. Eds. Rey, L.; May, J. C. Marcel Dekker: New York, 2004.
97. Patel, S. M.; Nail, S. L.; Pikal, M. J.; Geidobler, R.; Winter, G.; Hawe, A.; Davagnino, J.; Rambhatla Gupta, S., Lyophilized Drug Product Cake Appearance: What Is Acceptable? *Journal of Pharmaceutical Sciences* **2017**, *106* (7), 1706-1721.
98. Ciużyńska; Lenart, A., Freeze-Drying - Application in Food Processing and Biotechnology - A Review. *Polish Journal of Food and Nutrition Science* **2011**; Vol. 61.
99. Teagarden, D. L.; Baker, D. S., Practical aspects of lyophilization using non-aqueous co-solvent systems. *European Journal of Pharmaceutical Sciences* **2002**, *15* (2), 115-133.
100. Kunz, C.; Schuldt-Lieb, S.; Gieseler, H., Freeze-Drying From Organic Co-Solvent Systems, Part 2: Process Modifications to Reduce Residual Solvent Levels and Improve Product Quality Attributes. *Journal of Pharmaceutical Sciences* **2019**, *108* (1), 399-415.
101. Kunz, C.; Gieseler, H., Factors Influencing the Retention of Organic Solvents in Products Freeze-Dried From Co-Solvent Systems. *Journal of Pharmaceutical Sciences* **2018**, *107* (8), 2005-2012.
102. Kunz, C.; Schuldt-Lieb, S.; Gieseler, H., Freeze-Drying From Organic Cosolvent Systems, Part 1: Thermal Analysis of Cosolvent-Based Placebo Formulations in the Frozen State. *Journal of Pharmaceutical Sciences* **2018**, *107* (3), 887-896.
103. Gutiérrez, M. C.; Ferrer, M. L.; Mateo, C. R.; del Monte, F., Freeze-Drying of Aqueous Solutions of Deep Eutectic Solvents: A Suitable Approach to Deep Eutectic Suspensions of Self-Assembled Structures. *Langmuir* **2009**, *25* (10), 5509-5515.
104. Kasraian, K.; Deluca, P. P., Thermal-Analysis of the Tertiary Butyl Alcohol-Water System and Its Implications on Freeze-Drying. *Pharmaceutical Research* **1995**, *12* (4), 484-490.
105. Hanif, Z.; Jeon, H.; Tran, T. H.; Jegal, J.; Park, S. A.; Kim, S. M.; Park, J.; Hwang, S. Y.; Oh, D. X., Butanol-mediated oven-drying of nanocellulose with enhanced dehydration rate and aqueous re-dispersion. *Journal Polymer Research* **2017**, *25* (3).

106. Buckton, G., Contact angle, adsorption and wettability — a review with respect to powders. *Powder Technology* **1990**, *61* (3), 237-249.
107. Huhtamäki, T.; Tian, X.; Korhonen, J. T.; Ras, R. H. A., Surface-wetting characterization using contact-angle measurements. *Nature Protocols* **2018**, *13* (7), 1521-1538.
108. Bormashenko, E.; Gendelman, O.; Whyman, G., Superhydrophobicity of Lotus Leaves versus Birds Wings: Different Physical Mechanisms Leading to Similar Phenomena. *Langmuir* **2012**, *28* (42), 14992-14997.
109. Zheng, Q.; Lü, C., Size Effects of Surface Roughness to Superhydrophobicity. *Procedia IUTAM* **2014**, *10*, 462-475.
110. Xue, X.; Yang, Z.; Li, Y.; Sun, P.; Feng, Y.; He, Z.; Qu, T.; Dai, J.-G.; Zhang, T.; Qin, J.; Xu, L.; Zhang, W., Superhydrophobic self-cleaning solar reflective orange-gray paint coating. *Solar Energy Materials and Solar Cells* **2018**, *174*, 292-299.
111. Lai, Y.; Tang, Y.; Gong, J.; Gong, D.; Chi, L.; Lin, C.; Chen, Z., Transparent superhydrophobic/superhydrophilic TiO₂-based coatings for self-cleaning and anti-fogging. *Journal of Materials Chemistry* **2012**, *22* (15), 7420-7426.
112. Dong, H.; Cheng, M.; Zhang, Y.; Wei, H.; Shi, F., Extraordinary drag-reducing effect of a superhydrophobic coating on a macroscopic model ship at high speed. *Journal of Materials Chemistry A* **2013**, *1* (19), 5886-5891.
113. Jeevahan, J.; Chandrasekaran, M.; Joseph, G. B.; Durairaj, R. B.; Mageshwaran, G., Superhydrophobic surfaces: a review on fundamentals, applications, and challenges. *Journal of Coatings Technology and Research* **2018**, *15* (2), 231-250.
114. Blossey, R., Self-cleaning surfaces — virtual realities. *Nature Materials* **2003**, *2*, 301.
115. Wenzel, R. N., Resistance of Solid Surfaces to Wetting by Water. *Industrial & Engineering Chemistry* **1936**, *28* (8), 988-994.
116. Cassie, A. B. D.; Baxter, S., Wettability of porous surfaces. *Transactions of the Faraday Society* **1944**, *40* (0), 546-551.
117. Song, J., Rojas O., Approaching super-hydrophobicity from cellulosic materials: A Review. *Nordic Pulp and Paper Research Journal* **2013**; Vol. 28, p 216-238.
118. Almeida, A. P. C.; Canejo, J. P.; Fernandes, S. N.; Echeverria, C.; Almeida, P. L.; Godinho, M. H., Cellulose-Based Biomimetics and Their Applications. *Advanced Materials* **2018**, *30* (19), 1703655.
119. Huang, J.; Lyu, S.; Fu, F.; Chang, H.; Wang, S., Preparation of superhydrophobic coating with excellent abrasion resistance and durability using nanofibrillated cellulose. *RSC Advances* **2016**, *6* (108), 106194-106200.

120. Zheng, X.; Fu, S., Reconstructing micro/nano hierarchical structures particle with nanocellulose for superhydrophobic coatings. *Colloids and Surfaces A: Physicochemical and Engineering Aspects* **2019**, *560*, 171-179.
121. Teisala, H.; Tuominen, M.; Kuusipalo, J., Superhydrophobic Coatings on Cellulose-Based Materials: Fabrication, Properties, and Applications. *Advanced Materials Interfaces* **2014**, *1* (1), 1300026.
122. Kaushik, M.; Moores, A., Review: nanocelluloses as versatile supports for metal nanoparticles and their applications in catalysis. *Green Chemistry* **2016**, *18* (3), 622-637.

VITA

Miran Mavlan was born in Ghulja (Ili) in People's Republic of China. He immigrated to the United States to rejoin with his mother, father and brother in 1991. He attended Grover Cleveland High School where he graduated with honors in the Magnet Program with focus on philosophy and literature. Upon entering California State University, Northridge (CSUN) he pursued studies in in biochemistry and biomedical physics and earned his bachelor degree in 2010. During his undergraduate he was treasurer of the Muslim Student Association and president of the Uyghur Rights Association. After gaining some experience in industry working for Biocell Inc. (Torrance, CA) as a process and quality control chemisty he continued his studies with focus on organic chemistry at CSUN. In 2014 he earned his Masters under the tutelage of Thomas Minehan in the area of total synthesis and methodology development in glycosidic bond formations. In August 2015 he started his Ph.D. studies at Purdue University under the guidance of Alexander Wei in the areas of mechanochemistry and nanocellulose material reasearch until the completion of his doctorate degree.

PUBLICATIONS

Preprint

Quantitative Analysis of Oligosaccharides and Related Impurities in Cellulose Nanocrystals

Francisco J. Montes^{1,a}, Miran Mavlan^{2,a}, Reaz Chowdhury^{1,a}, Iman Beheshti Tabar³, Alexander Wei^{2,*}, Jeffrey P. Youngblood^{1,*}

¹ School of Materials Science and Engineering, Purdue University, West Lafayette, IN 47907

² Department of Chemistry, Purdue University, West Lafayette, IN 47907

³ Laboratory of Renewable Resources Engineering and Department of Agricultural and Biological Engineering, Purdue University, West Lafayette, IN 47907

^a These authors had equal contributions to this manuscript.

ABSTRACT:

The presence of soluble carbohydrate derivatives in cellulose nanocrystal (CNC) slurries is an uncontrolled variable that can significantly alter the properties of CNC-based materials and compromise subsequent performance. In this work, the content of soluble carbohydrates in CNC slurries from nine independent samples has been characterized and classified by sugar type and size, with large variations due to differences in plant source, process, and purification methods. Analytical methods include anthrone and bicinchoninic acid (BCA) tests for estimating reducing-end sugar and total sugar content, HPLC to determine the relative fraction of mono- and oligosaccharides, and MALDI/TOF for oligosaccharide analysis. The quantity and type of soluble carbohydrates in a given CNC slurry varies widely with plant origin and methods of CNC production and purification, as well as sample age. While the fraction of soluble carbohydrates can

be partially reduced by ultrasonication and ultrafiltration, extensive washing is not sufficient for their complete removal. This suggests that the residual carbohydrates are strongly bound to CNCs, or easily regenerated upon ultrasonication.

Keywords:

Oligosaccharides, Cellulose Nanocrystals, Impurities, Sugar Detection.

In the anthrone assay, dilute solutions of oligo- and polysaccharides are rapidly hydrolyzed into free sugars, which undergo further dehydration and condensation with anthrone to produce a blue-green solution with an absorbance peak at 630 nm (Figure 1). The assay is complete within minutes and provides a convenient method for estimating the total concentration of free sugars (mostly glucose units) in CNC samples. We note that non-reducing sugar alcohols cannot be accounted for by the anthrone assay, however these are not expected to be significant based on the process chemistry used to produce CNC samples. However, the CNCs themselves can degrade further under strongly acidic conditions, so their removal by sedimentation or ultrafiltration prior to the anthrone assay is important.

Estimates of soluble reducing sugar in the filtrates of CNC samples (diluted 10X) were calibrated against a standard curve prepared with dextrose. Absorbance values ranged from 0.69 (CNC4) to 0.01 (CNC6), corresponding to total sugar (glucose) concentrations from 925 to 2 mg/mL, respectively (Figure 1a). The following outcomes were noted:

- (i) Residual sugar content in CNCs derived from different wood and plant sources varied widely, even when purified using similar methods (CNC1, CNC2, CNC6, CNC7).
- (ii) Samples from the same wood source but different lots (CNC1, CNC2) also showed large variations, indicating low control during the degradation or purification process.
- (iii) The amount of soluble sugar increased/remained constant over time (CNC2a, CNC2b).

- (iv) Residual sugar content decreased in accord with the method of purification used, based on overall dilution factor. For example, CNC4 was subjected to XX rounds of ultrafiltration (dilution factor = 11^{XX}), whereas CNC3 and CNC5 were subjected to XX rounds of sedimentation and ultrafiltration, respectively (dilution factors = XXX and XXX).
- (v) Oxidative methods for CNC processing correlated with higher residual sugar content (CNC8, CNC9), however the relationship is tenuous as different plant sources and purification methods are also factors.

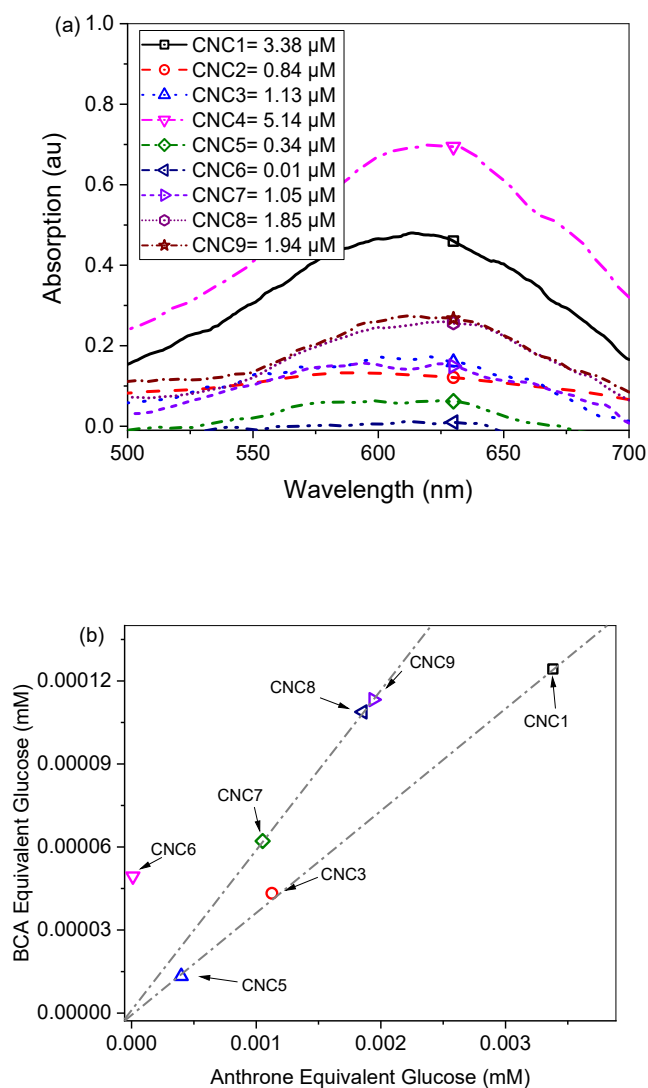


Figure 1. (a) Anthrone assay estimating total sugar (glucose equivalent, mM) in filtrates collected from CNC1–CNC9 (see Table 1), following a 10X dilution. (b) Estimates of total sugars (anthrone assay) versus soluble reducing-end sugar (modified BCA assay), with linear correlations (lines drawn to guide the eye) fits the proportion of the total sugar rings detected and the sugar rings with a reducing end. **Data for CNC2 and CNC4 not included.**

With regard to the impact of purification methods on the removal of residual sugars, multiple rounds of sedimentation (by centrifugation, method B) appears to be more efficient than passive filtration by membrane dialysis (method D). This indicates that additional oligosaccharides are likely removed from CNCs by shear forces during centrifugation. However, sedimentation can be laborious and time-consuming, and cannot be easily performed on an industrial scale. Very importantly, the difference in free sugar content between CNC filtrates obtained by methods B and D has no correlation with ionic conductivity (2 mS/cm versus 50 μ S/cm, respectively). Therefore, reductions in residual sugar concentration after each purification step cannot be based on simple dilution factors, due to their gradual dissociation from CNCs.

As mentioned earlier, the strongly acidic conditions of the anthrone test is expected to hydrolyze the glycosidic bonds of all soluble oligosaccharides, yielding an estimate of total free sugar (glucose units) in the filtrate following acid digestion. To quantify the concentration of reducing-end sugars (mixture mono- and oligosaccharides) under non-hydrolytic conditions, all CNC filtrate samples were subjected to the modified BCA assay under the assumption that cross-reactive species such as peptides were absent. The effective concentrations of soluble sugars were calibrated against a dextrose standard, and presented as reducing-end units for comparison with data from the anthrose assay (Figure 1b and Table 2).

Table 2. Estimates of soluble reducing sugars in filtrates using the modified BCA assay.

Sample ID	Solute (units?) ^a	Reducing-end units (μmol/mL) ^b	Glucose Equivalent (mg/L) ^b
CNC1	3.6	124.3	22.4
CNC2			
CNC3	5.0	43.2	7.8
CNC4			
CNC5	2.9	13.5	2.4
CNC6	15.6	49.7	8.9
CNC7	4.8	62.3	11.2
CNC8	2.3	108.7	19.6
CNC9	6.9	113.5	20.4

^a Final concentration of filtrate after dilution. ^b Mean of XX measurements.

As expected, the concentration of reducing-end sugars scales with that of total glucose units estimated by the anthrone assay, in a roughly linear fashion (Figure 1). The ratio of the two values depends partly on the plant source: filtrates from wood-derived CNCs (CNC1–CNC5) exhibit ratios that indicate most of the soluble sugar to exist in polysaccharide form with an average degree of polymerization (DP) of 27, whereas those from other plant sources (CNC7–CNC9) yield mean DP values closer to 17. CNC6 is a noteworthy exception with a mean DP value of 0.2, a strong indication that longer oligosaccharides were largely absent. Given the nonspecific nature of the BCA assay it is possible that this measurement is artificially boosted by plant proteins or other impurities[28], [29], however we have no indicators that further support this notion.

HPLC analysis provided some additional insights into the residual sugars from various CNC filtrates (Figure 2). While all filtrates contained glucose as expected, the chromatographs were in fact dominated by oligo- and polysaccharides (DP > 2), whose retention times were too short to permit the identification of specific oligomers using the available column and method. Indeed, only one sample (CNC8) produced peaks suggesting a significant fraction of cellobiose.

Several samples also contained minor amounts of solutes having higher polarity, suggestive of organic acids generated during the oxidative degradation of glucose[1]; further analysis of these byproducts was not pursued. Lastly, other plant-derived monosaccharides such as xylose and arabinose were not observed in significant quantities. Overall, the HPLC analysis qualitatively confirms our earlier observation that most of the soluble sugar in CNC filtrates exists in the form of oligo- and polysaccharides.

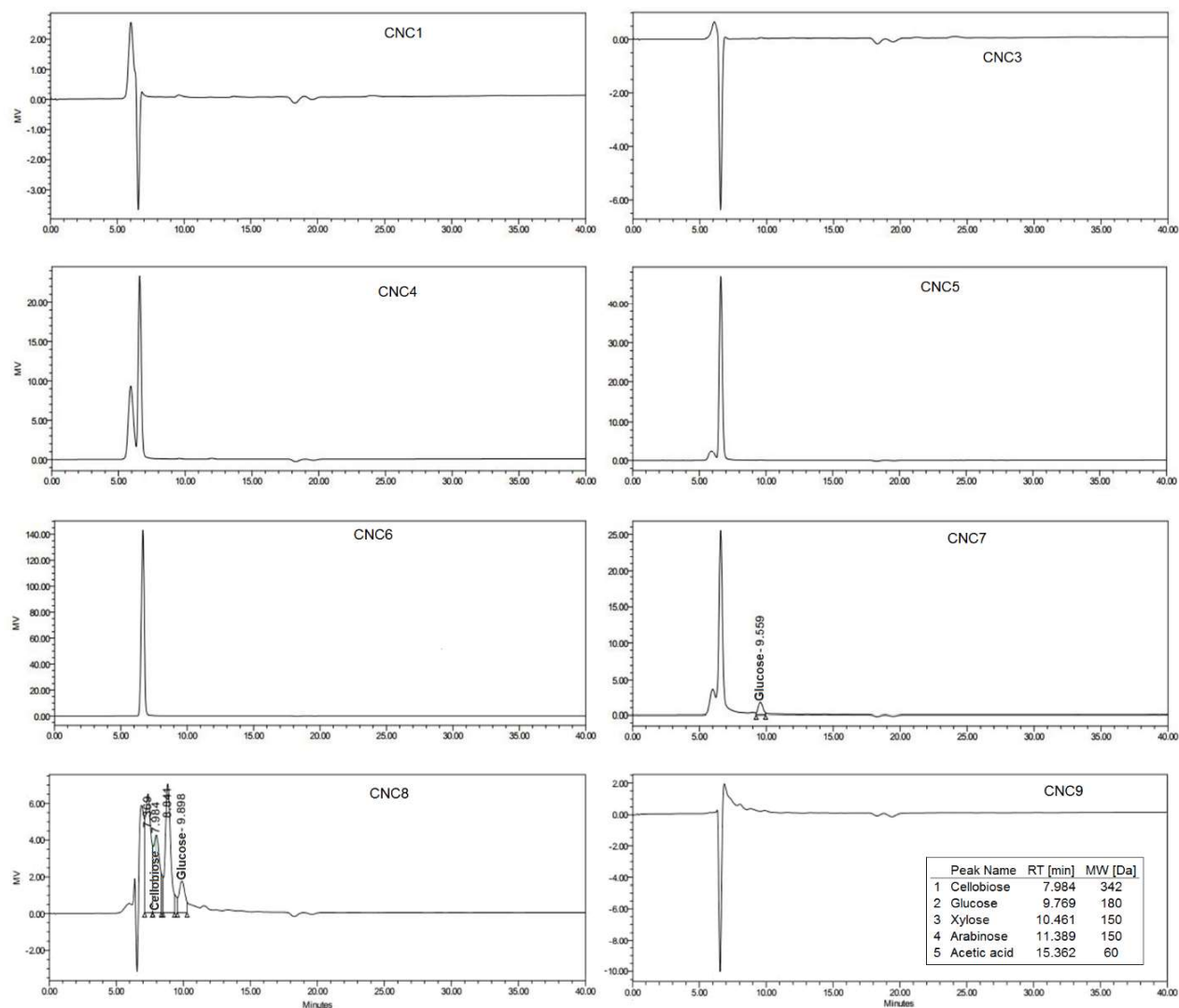


Figure 2. HPLC analysis of CNC filtrates. Peaks with retention times similar to known molecules are indicated. Retention times of some standard compounds are provided for comparison (*inset*, lower right). MV = ??

Two HPLC samples contained sufficient quantities of free sugar to merit further analysis. The filtrate from CNC7 contained significant levels of residual glucose, estimated at 77 mg/L (0.43 μ M); the filtrate from CNC8 contained glucose and also cellobiose, estimated at 234 mg/L (1.3 μ M). These values corresponded respectively to 40% and 70% of the reducing-end sugars plotted

in **Error! Reference source not found.** The relatively high estimate for CNC8 can be attributed to the oxidative degradation of oligosaccharides during the CNC production process.

CNC filtrates were also subjected to MS analysis using MALDI-TOF to characterize the molecular weights of residual sugars present in relatively high abundance. The most prevalent MS peaks were found between m/z 200 and 800, with the four most common ions having m/z values of 273, 372, 413 and 551 (Figure 3). For comparison, the molecular weights of oligocelluloses are 342, 504, and 666 Da (DP2, DP3, and DP4 respectively). Higher molecular-weight species were not observed, most likely due to their lower solubility or dispersion in the organic matrix relative to low molecular-weight derivatives [30]. It is worth noting that synthetic oligocellulose with DP > 20 have been evaluated by MALDI-TOF analysis[31], indicating that further effort may be needed to release residual oligosaccharides from CNC filtrates into well-dispersed forms. Nevertheless, the MS data provided here is sufficient to establish that the residual sugar content is comprised of more than simple mono- or disaccharides, in accord with the colorimetric assays.

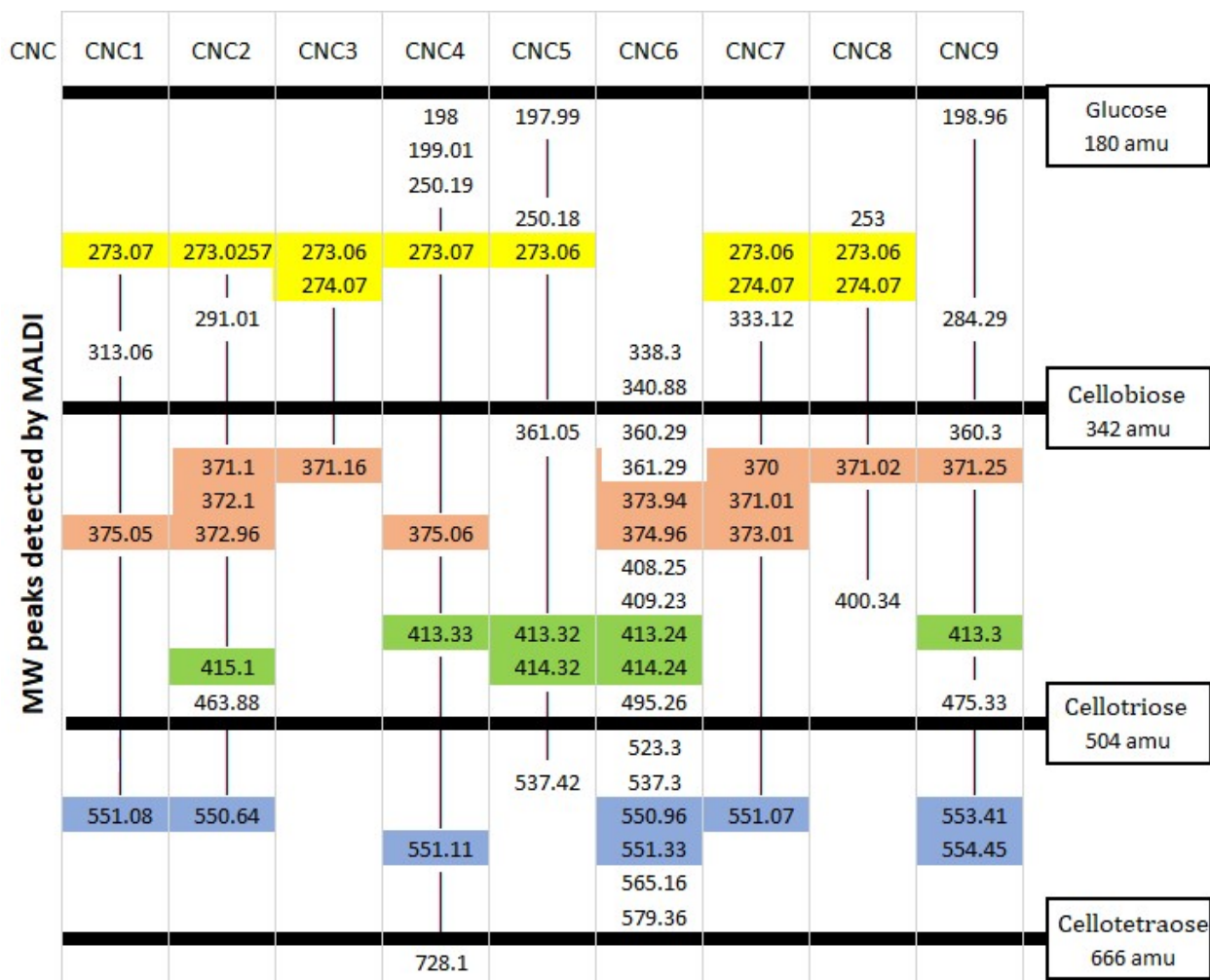


Figure 3. MALDI-TOF results of CNC filtrates; ions with common m/z values are highlighted. Heavy horizontal lines correspond to oligocelluloses with similar molecular weights (in amu).

Tandem mass spectrometry (MS/MS) was performed on selected ions to gain further insights into the fine structure of the more populous ions; their corresponding fragment ions are listed in Figure 5. Given the original assumption that the molecules we are seeing are polysaccharides, the NIST Chemistry WebBook[32] was used to narrow the obtained molecular weights to documented carbohydrates. However, the combinations would be endless, as there are hundreds of documented carbohydrates with each of the obtained molecular weights. Despite the complication, there are a couple interesting observations within the 273-274 ions: While there was

no C-H-O molecule that matched the 273 or 274 molecular weights, if nitrogen was added to the formula, several matches (aminoacids, nitrates, and nitrate esters) appeared. Although the origin of aminoacids or even the mere presence of nitrogen in these materials is not clear, these are two more examples of the possibilities mentioned at the end of section 3.2, where a molecule could be detected by BCA, but not by anthrone assay.

Sample Name	CNC4	CNC1	CNC3	CNC2
Selected Molecular Weight [amu]	273	372	413	551
MS/MS detected Fragments [amu]	136	10	112	154
	137	173	140	159
	Dextrose MW 180 amu			
		198		238

Figure 10 MS/MS Result from selected MALDI Ions. Dextrose is pointed out to show the proximity of the detected fragments to a single ring saccharide.

Once again, the results obtained by MS/MS did not match the expected single ring molecular weight, but yielded unexpected values around it. Taking into account the different measured characteristics of the detected impurities, finding an exact match for the molecules detected by MALDI that could also break into the fragments detected by MS/MS, with the same retention times as the molecules detected by HPLC, would be not only be time consuming but improbable. On the other hand, if the CNC are going to be used in an application concerned by the presence of specific molecules, with MALDI responses similar to the detected ions, and links of the size of the fragments detected by MS/MS, the combination of these two methods could be useful to confirm its presence.

Table 4 Information obtained in this work.

Question	Method and Answer
Is there a fast and easy method to measure free sugars?	Anthrone assay provides a fast, reliable and inexpensive method for oligosaccharide detection in CNC filtrates.
How many reducing sugars?	BCA detected different concentrations of reducing ends for each sample, however, no information about the rest of the molecule is provided by these results. A concentration can be inferred if glucose molecules are assumed.
What determines the sugars content?	Anthrone assay showed the amount of free sugars in the filtrates could be related to aging, production and purification method.
Are there any known sugars?	HPLC detected very few of the suspected saccharides, most of the molecules detected had a retention time characteristic of molecules larger than a disaccharide.
Exactly how big are they?	MALDI detected several ions in the range of one to four sugar rings. No exact match of a traditional oligosaccharide was found. However, the same four ions were detected in almost all the samples tested.
Can single rings be obtained through fragmentation?	MS/MS showed how the previously detected ions fragmented into two or three smaller molecules. No fragment was an exact match for a single glucose ring.
Can the impurities be washed away?	Ultrasonication and Ultrafiltration can be used several times to reduce the amount of impurities in the CNC slurries. It is possible that impurities keep appearing after several washes due to amorphous regions being cleaved from the crystalline domains.

This work originated from the suspicion of the existence of impurities in the form of free sugars in the CNC slurries. After the CNC were separated from the continuous media by ultrafiltration through a 300 kDa membrane, several chemical assays were conducted to confirm the existence of carbohydrate contaminants in the CNC slurries. Chemical methods also helped to characterize the impurities and provided valuable information about their nature.

It was found that there were free reducing sugars in the slurries, but also other oligosaccharides were detected, so a more comprehensive technique than a simple sugar test or a conductivity measurement is needed to detect and quantify these contaminants. Anthrone assay proved to be useful tool for determining the content of carbohydrate contaminants.

The exact determination of the nature of the polysaccharides is very difficult, although, the amount of detected polysaccharides by anthrone assay were small (under 0.1wt%). If the desired application demands a high purity, or if it requires the absence of a particular component with a known response to the methods presented in this work, impurities can be washed away extensive ultrafiltration. However, the impurities appeared to be bound to the CNC and it should not assumed or expected that these impurities would come out as easy or fast as glucose or salts. Thus, purification of CNCs during production to a conductivity end-point may leave significant polysaccharide in the material, and as such a separate anthrone endpoint should also be instituted, depending on the application.

Acknowledgements

The authors would like to thank the National Science Foundation Scalable Nanomanufacturing program under award CMMI-1449358 and the US Endowment for Forestry and Communities Grant P3-1 for funding this research. We also want to thank Alan Rudie from the USFS Forest Products Laboratory and Sean McAlpine from Blue Goose Biorefineries Inc. for sharing their knowledge and providing the CNC materials for this work.

References

- [1] R. J. Moon, A. Martini, J. Nairn, J. Simonsen, and J. Youngblood, "Cellulose nanomaterials

- review: Structure, properties and nanocomposites,” *Chem. Soc. Rev.*, vol. 40, no. 7, pp. 3941–3994, Jul. 2011.
- [2] J. A. Diaz *et al.*, “Thermal Conductivity in Nanostructured Films: From Single Cellulose Nanocrystals to Bulk Films,” 2014.
- [3] R. R. Lahiji, X. Xu, R. Reifenberger, A. Raman, A. Rudie, and R. J. Moon, “Atomic Force Microscopy Characterization of Cellulose Nanocrystals,” *Langmuir*, vol. 26, no. 6, pp. 4480–4488, 2010.
- [4] M. Nogi, S. Iwamoto, A. N. Nakagaito, and H. Yano, “Optically Transparent Nanofiber Paper,” *Adv. Mater.*, vol. 21, no. 16, pp. 1595–1598, 2009.
- [5] A. Dufresne, *Nanocellulose: From Nature to High Performance Tailored Material*, De Gruyter., vol. 67, no. 3. ProQuest Ebook Central, 2013.
- [6] R. A. Chowdhury *et al.*, “Self-healing epoxy composites: Preparation, characterization and healing performance,” *J. Mater. Res. Technol.*, vol. 4, no. 1, pp. 33–43, 2015.
- [7] Y. Zhou *et al.*, “Recyclable organic solar cells on cellulose nanocrystal substrates,” *Sci. Rep.*, vol. 3, p. 1536, Mar. 2013.
- [8] T. Fu, F. Montes, P. Suraneni, J. Youngblood, and J. Weiss, “The Influence of Cellulose Nanocrystals on the Hydration and Flexural Strength of Portland Cement Pastes,” *Polymers (Basel)*, vol. 9, no. 9, p. 424, 2017.
- [9] W. Li, R. Guo, Y. Lan, Y. Zhang, W. Xue, and Y. Zhang, “Preparation and properties of cellulose nanocrystals reinforced collagen composite films,” *J. Biomed. Mater. Res. Part A*, vol. 102, no. 4, pp. 1131–1139, 2014.
- [10] J. P. F. Lagerwall, C. Schutz, M. Salajkova, J. Noh, J. H. Park, and C. Schu, “Cellulose nanocrystal-based materials : from liquid crystal self-assembly and glass formation to

- multifunctional thin films,” no. October 2013, pp. 1–12, 2014.
- [11] Y. Cao *et al.*, “The influence of cellulose nanocrystals on the microstructure of cement paste,” *Cem. Concr. Compos.*, vol. 74, pp. 164–173, 2016.
- [12] T. Fu, R. J. Moon, P. Zavattieri, J. Youngblood, and W. J. Weiss, “Cellulose nanomaterials as additives for cementitious materials,” *Cellul. Nanofibre Compos. Prod. Prop. Appl.*, vol. C, pp. 455–482, 2017.
- [13] Y. Cao, P. Zavattieri, J. Youngblood, R. Moon, and J. Weiss, “The influence of cellulose nanocrystal additions on the performance of cement paste,” *Cem. Concr. Compos.*, vol. 56, pp. 73–83, 2015.
- [14] M. Bishop and A. R. Barron, “Cement hydration inhibition with sucrose, tartaric acid, and lignosulfonate: Analytical and spectroscopic study,” *Ind. Eng. Chem. Res.*, vol. 45, no. 21, pp. 7042–7049, 2006.
- [15] L. Zhang, L. J. J. Catalan, R. J. Balec, A. C. Larsen, H. H. Esmaeili, and S. D. Kinrade, “Effects of saccharide set retarders on the hydration of ordinary portland cement and pure tricalcium silicate,” *J. Am. Ceram. Soc.*, vol. 93, no. 1, pp. 279–287, 2010.
- [16] C. Y. Wang *et al.*, “Stable low-voltage operation top-gate organic field-effect transistors on cellulose nanocrystal substrates,” *ACS Appl. Mater. Interfaces*, vol. 7, no. 8, pp. 4804–4808, 2015.
- [17] S. McAlpine and J. Nakoneshny, “WO 2017/127938 A1,” 2017.
- [18] A. A. Olkowski, B. Laarveld, and N. Arrison, “US 9,388,251 B2,” 2016.
- [19] G. L. Miller, “Use of Dinitrosalicylic Acid Reagent for Determination of Reducing Sugar,” *Anal. Chem.*, vol. 31, no. 3, pp. 426–428, 1959.
- [20] W. Z. Hassid and S. Abraham, “[7] Chemical procedures for analysis of polysaccharides,”

- Methods Enzymol.*, vol. 3, no. C, pp. 34–50, 1957.
- [21] A. A. Albalasmeh, A. A. Berhe, and T. A. Ghezzehei, “A new method for rapid determination of carbohydrate and total carbon concentrations using UV spectrophotometry,” *Carbohydr. Polym.*, vol. 97, no. 2, pp. 253–261, 2013.
- [22] S. KONGRUANG, M. J. HAN, C. I. GIL BRETON, and M. H. PENNER, “Quantitative Analysis of Cellulose-Reducing Ends,” *Appl. Biochem. Biotechnol.*, vol. 113–116, pp. 213–231, 2004.
- [23] S. Waffenschmidt and L. Jaenicke, “Assay of Reducing Sugars in the Nanomole Range with 2, 2’ -Bicinchoninate,” *Anal. Biochem.*, vol. 165, pp. 337–340, 1987.
- [24] S. Ori, A., Shinkai, “Electrochemical detection of saccharides by the redox cycle of a chiral ferrocenylboronic acid derivative: a novel method for sugar sensing,” *J. Chem. Soc. Chem. Commun.*, vol. 645, no. March, pp. 1771–1772, 1995.
- [25] G. A. Grant, S. L. Frison, T. Yeung, T. Vasanthan, and P. Sprons, “Comparison of MALDI-TOF Mass Spectrometric to Enzyme Colorimetric Quantification of Glucose from Enzyme-Hydrolyzed Starch,” *Agric. Food Chem.*, vol. 51, pp. 6137–3144, 2003.
- [26] M. Karas and F. Hillenkamp, “Laser Desorption Ionization of Proteins with Molecular Masses Exceeding 10 000 Daltons,” *Anal. Chem.*, vol. 60, no. 20, pp. 2299–2301, 1988.
- [27] Y. H. P. Zhang and L. R. Lynd, “Determination of the number-average degree of polymerization of cellodextrins and cellulose with application to enzymatic hydrolysis,” *Biomacromolecules*, vol. 6, no. 3, pp. 1510–1515, 2005.
- [28] K. J. Wiechelman, R. D. Braun, and J. D. Fitzpatrick, “Investigation of the bicinchoninic acid protein assay: Identification of the groups responsible for color formation,” *Anal. Biochem.*, vol. 175, no. 1, pp. 231–237, 1988.

- [29] N. E. Maurer, B. Hatta-Sakoda, G. Pascual-Chagman, and L. E. Rodriguez-Saona, "Characterization and authentication of a novel vegetable source of omega-3 fatty acids, sacha inchi (*Plukenetia volubilis* L.) oil," *Food Chem.*, vol. 134, no. 2, pp. 1173–1180, 2012.
- [30] D. J. Harvey, "Derivatization of carbohydrates for analysis by chromatography; electrophoresis and mass spectrometry & , &&," *J. Chromatogr. B*, vol. 879, no. 17–18, pp. 1196–1225, 2011.
- [31] D. M. Petrovic, I. Kok, A. J. J. Woortman, C. Jelena, and K. Loos, "Characterization of Oligocellulose Synthesized by Reverse Phosphorolysis Using Different Cellodextrin Phosphorylases," 2015.
- [32] NIST, "NIST Chemistry WebBook," *Chemistry WebBook*, 2017. [Online]. Available: <http://webbook.nist.gov/chemistry/mw-ser/>. [Accessed: 20-Jun-2017].